Master's thesis

NTNU
Norwegian University of Science and Technology

Adrian Hansø

ROV-based *in situ* monitoring of cultivated kelp biomass using underwater RGB images and the Segment Anything Model

Master's thesis in Ocean Resources
Supervisor: Glaucia M. Fragoso
Co-supervisor: Phil Tinn, David Aldridge, Geir Johnsen

May 2024

NTNU
Norwegian University of
Science and Technology

Adrian Hansø

ROV-based *in situ* monitoring of cultivated kelp biomass using underwater RGB images and the Segment Anything Model

Master's thesis in Ocean Resources
Supervisor: Glaucia M. Fragoso
Co-supervisor: Phil Tinn, David Aldridge, Geir Johnsen
May 2024

Norwegian University of Science and Technology

NTNU
Norwegian University of
Science and Technology

Abstract

Seaweed cultivation is increasingly recognised for its potential to support the bioeconomy and reduce our dependence on fossil fuels. Over the past two decades, the industry has experienced rapid growth, with a tripling in production volumes. Norway's seaweed cultivation sector possesses ideal conditions for industrialising and scaling up production. However, achieving this requires automated monitoring techniques to manage large-scale production effectively. The recent availability of low-cost underwater vehicles, coupled with significant advancements in machine learning-based image processing, has the potential to revolutionise underwater monitoring in the near future.

In this study, we investigate *in situ* biomass monitoring of cultivated *Saccharina latissima* canopies using underwater red-green-blue (RGB) imaging and the Segment Anything Model (SAM), a state-of-the-art foundation model for image segmentation. To achieve this, we utilised a mini- remotely operated vehicle (ROV) for image sampling of side and top-down views of vertically-oriented canopies growing along horizontally-oriented cultivation lines. The SAM was used to segment a small section of the canopy, for its pixel area to be spatially calibrated to area estimations in in dm^2 m^{-1} and correlated with field-measured biomass. *In situ* chlorophyll *a* concentrations and turbidity (proxies for phytoplankton biomass and particle concentrations) were monitored to evaluate and quantify their impact on image quality and canopy segmentation accuracy.

The side view area proved to be a robust proxy for biomass, showing a strong positive power relationship (r^2 = 0.769). The top-down view area demonstrated a noticeably weaker power relationship with biomass (r^2 = 0.365). However, the top-down view area demonstrated a strong power relationship to sporophyte density (r^2 = 0.676), indicating that canopy width correlates well with sporophyte distribution along the cultivation line.

Our work extends previous research that employed conventional segmentation techniques, such as shift clustering, colour segmentation and adaptive thresholding, for kelp canopy area segmentation. The SAM consistently achieved high accuracy in segmenting the kelp canopies, even from substantially degraded images. Our findings indicate that a foundation model for image segmentation like the SAM enhances the adaptability, efficiency, and accuracy of canopy segmentations compared to conventional segmentation techniques. To further improve accuracy and minimise the need for manual supervision, the SAM can be fine-tuned specifically for kelp canopy segmentations in the waters of Frøya. For this purpose, we have released together with this thesis our dataset of 108 canopy replicate images and their corresponding segmentations.

Our findings support evidence that area estimations from underwater imagery of kelp canopies can serve as a robust proxy for canopy biomass. This demonstrates the future potential of deriving structural canopy metrics from underwater imaging to offer new insights into *S. latissima* distribution and growth patterns. Our work presents a novel step toward automated, large-scale, *in situ* monitoring of cultivated kelp canopies. However, our current approach faces several constraints, such as operational limitations in the field and semi-automatic processing. We envision that our work can serve as a foundation for overcoming these limitations by implementing autonomous sensory systems and advanced machine learning processing.

Sammendrag

Dyrking av tang og tare anerkjennes i økende grad for sitt potensial til å bidra til bioøkonomien og redusere vår bruk av fossile brensler. I løpet av de siste to tiårene har industrien opplevd en hurtig vekst, med en tredobling i produksjonsvolum. Norges taredyrkingssektor har ideelle forhold for å industrialisere og skalere opp produksjonen. For å oppnå dette er det imidlertid nødvendig med automatiserte overvåkningsteknikker for å effektivt håndtere en storskala produksjon. Den nye tilgjengeligheten på rimelige undervannsfarkoster, kombinert med betydelige fremskritt innen maskinlæringsbasert bildebehandling, har potensial til å revolusjonere undervannsovervåkning i nær fremtid.

I dette studiet undersøker vi *in situ* biomasseovervåkning av den dyrkede taren *Saccharina latissima* ved bruk av undervanns rød-grønn-blå (RGB) bilder og Segment Anything Model (SAM), en banebrytende modell for bildesegmentering. For å oppnå dette brukte vi en fjernstyrt undervannsfarkost (ROV) for å samle bilder av side- og ovenfra-ned-perspektiv på vertikalt orienterte tare som vokser langs horisontalt orienterte dyrkingsliner. SAM ble brukt til å segmentere en liten replika av taren på dyrkningslinjen, slik at pikselområdet kunne omgjøres til arealestimater i $dm^2\ m^{-1}$ og korreleres med feltmålt biomasse. *In situ* konsentrasjoner av klorofyll *a* og turbiditet (proxy for fytoplanktonbiomasse og partikkelkonsentrasjon) ble overvåket for å evaluere og kvantifisere deres innvirkning på bildekvalitet og nøyaktighet av tare-segmentering.

Side-perspektiv arealet viste seg å være en robust proxy for biomasse, med en sterk positiv potensrelasjon (r^2 = 0,769). Ovenfra-ned-perspektivet viste en merkbart svakere potensrelasjon med biomasse (r^2 = 0,365). Imidlertid viste topp-ned-arealet en sterk potensrelasjon til sporofytt-tetthet (r^2 = 0,676), noe som indikerer at tareformasjonens bredde korrelerer godt med sporofyttfordelingen langs dyrkningsliner.

Vårt arbeid viderefører tidligere forskning som brukte konvensjonelle segmenteringsteknikker for å tare-segmentering. SAM oppnådde konsekvent høy nøyaktighet i segmenteringen av tareveksten, selv fra vesentlig degraderte bilder. Våre funn indikerer at en grunnmodell for bildesegmentering, som SAM, forbedrer fleksibiliteten, effektiviteten og nøyaktigheten til tare-segmenteringer sammenlignet med konvensjonelle segmenteringsteknikker. For å ytterligere forbedre nøyaktigheten og minimere behovet for menneskelig tilsyn, kan SAM finjusteres spesifikt for tare-segmentering i havområdene rundt Frøya. Til dette formålet har vi utgitt vårt datasett med 108 dyrkningsline bilder med sine tilhørende segmenteringer sammen med denne avhandlingen.

Våre funn underbygger beviset på at arealestimater fra undervannsbilder av tarevekst kan fungere som en robust proxy for tarevekstbiomasse. Dette demonstrerer det fremtidige potensialet for å uthente strukturelle taremålinger fra undervannsbilder for å gi ny innsikt i *S. latissima*-distribusjon og vekstmønster. Vårt arbeid presenterer et skritt i retning automatisert, storskala, *in situ* overvåking av dyrket tare. Imidlertid står vår nåværende tilnærming overfor flere begrensninger, som operasjonelle restriksjoner i feltet og semi-automatisk prosessering. Vi ser for oss at vårt arbeid kan brukes som et grunnlag for å overvinne disse begrensningene ved å implementere autonome sensorsystemer og avansert maskinlæringsbehandling.

Acknowledgements

This MSc project has been completed at the Norwegian University of Science and Technology in the period from December 2022 to May 2024. The thesis was part of the following project: "Autonomous underwater monitoring of kelp-farm biomass, growth, health and biofouling using optical sensors", MoniTARE (315514) (2021-2025) and funded by the Research Council of Norway (RCN). Access to the kelp farm in Frøya was provided by Seaweed Solutions.

I would like to express my gratitude to my main supervisor, Glaucia Moreira Fragoso, for giving me the opportunity to be a part of this project. I have greatly appreciated your guidance, patience, and trust, which allowed me to explore my ideas and develop new skills throughout this research journey. I would also like to thank my co-supervisors, Phil Tinn, David Aldrige and Geir Johnsen, for their valuable insights and constructive feedback. Their contributions greatly enriched this research and helped me navigate various challenges along the way. Last but not least, my heartfelt thanks to the rest of the KELPie team, Els Snijder and Nalia Hama, my field partners in crime!

On a more personal note, I would like to extend my deepest gratitude to my friends and family. I am incredibly thankful for your constant belief in me and for reminding me to find time for life outside of my research. A special thanks to Karita Løken for always being there for me and Sebastian Gjertsen for his assistance with proofreading and providing moral support in all aspects of life.

Table of Contents

Abbreviations

AOP	Apparent optical properties
AUV	Autonomous underwater vehicles
cDOM	Coloured dissolved organic material
Chl *a*	Chlorophyll *a*
CV	Computer vision
CVAT	Computer Vision Annotation Tool
FTU	Formazin Turbidity Unit
IOP	Inherent optical properties
IoU	Intersection over Union
MI	Måskjæra Inside
NAC	Norwegian Atlantic Current
NCC	Norwegian Costal Current
PCA	Principal component analysis
R^2	Coefficient of determination
RGB	Red-Green-Blue
ROV	Remotely operated vehicles
SAM	Segment Anything Model
SES	Seaweed Solutions
TSM	Total suspended matter

1 Introduction

1.1 Seaweed aquaculture

Marine macroalgae (seaweeds) are multicellular aquatic photosynthetic organisms and the dominant primary producer in the coastal zone (Krause-Jensen & Duarte, 2016). Coastal communities have, for more than 10 000 years, been harvesting seaweed and using it for domestic purposes, such as food, feed and medicine (Dillehay et al., 2008). The use of seaweed is especially widespread in East Asia, where it has been an essential part of their cuisine for over a thousand years (Hwang et al., 2019). In addition to a long history of wild harvesting, East Asian countries have been pioneers in developing methodologies for seaweed cultivation over the last century, changing seaweed production from a simple collection of natural resources into an industrial farming industry. In combination with modern processing methods, seaweed is today utilised in sectors such as human food, livestock feed and renewable feedstocks (Yong et al., 2022).

As the world's population is rapidly growing, it remains a significant challenge to reduce the pressure on Earth's natural resources while at the same time supporting the increasing demand for energy and food (Davis et al., 2016; Lee et al., 2019). The flexibility of seaweed highlights its potential to support the growing bioeconomy by acting as a low-trophic-level feedstock and reducing our dependence on fossil fuels. Despite solid management strategies, wild seaweed resources will not be sufficient to meet this future demand (Steen et al., 2016; Monagail et al., 2017; Lauzon-Guay et al., 2021). Seaweed aquaculture, on the other hand, is gaining attention as a unique, scalable, and sustainable approach to this dilemma (Duarte et al., 2021). As evidenced in the newest seaweed market report from the World Bank (2023), the industry has significantly grown in the past two decades, with production volume tripling. The report further states that, as of 2020, global seaweed aquaculture produced 35.1 million tons of wet-weight biomass, accounting for nearly 30 percent of total aquaculture production. Despite of this high volume, seaweeds accounted for only 5.9% of aquaculture production value. In both volume and value, Asian producers dominate the seaweed market, holding over 98 % of the global market share (World Bank, 2023). Current production volumes outside of Asia are low, but a significant growth rate is predicted, particularly in parts of Europe and America, where industry, government, and academia are aligning their efforts (Kraan, 2020). The European Union refers to the algae sector as an "untapped resource" and considers it a key pillar in its blue bioeconomy strategy (European Commission, 2023). The UN Global Compact is going as far as calling it a "Seaweed Revolution" for the industry's potential to contribute to the United Nations Sustainable Development Goals (Lloyd's Register Foundation, 2020).

1.2 Seaweed aquaculture in Norway

Seaweed cultivation in Norway started on an experimental scale in 2005, with key stakeholders from research and private sectors collaborating to develop cultivation technology for scaling up biomass production (Stévant et al., 2017). The initial motivation for increasing production was to use kelp carbohydrates to produce biofuel. However, due to the high short-term production costs, using biomass solely for biofuel was deemed economically unachievable. Consequently, prioritising products that could generate economic viability in the short term was recommended as an initial step (Skjermo et al., 2014).

Seaweed cultivation in Norway is currently focused on two species of brown seaweed (*Phaeophyceae*), namely the kelp *Saccharina latissima* (sugar kelp) and *Alaria esculenta* (winged kelp), selected for their high biomass yields (Skjermo et al., 2014; Cai et al., 2021). Sales figures from 2022 indicate a total volume of 221 tons of wet weight, valued at NOK 4.2 million, comprising 161 tons of *S. latissima* and 60 tons of *A. esculenta* (Directorate of Fisheries, 2024). Biomass is primarily used for human consumption, but an increasing range of products are being developed, including animal feed, fertiliser, cosmetics and pharmaceuticals.

Norway's long coastline, favourable water conditions and leading expertise in marine operations provide excellent prerequisites for industrialising the seaweed cultivation industry (Skjermo et al., 2014). Although the Norwegian seaweed cultivation industry is still in its early stages, it has generated significant positive attention through optimistic policy narratives and media coverage (Albrecht & Lukkarinen, 2020). This optimism is further reinforced by several reports from Norwegian research institutes, which project a growth potential of annual production volumes of 20 million tons by 2050 (Olafsen et al., 2012; Skjermo et al., 2014; Broch et al., 2019), although there is some debate regarding the realism of these projections (Albrecht, 2023). Norwegian seaweed aquaculture has the potential to become a major contributor to the European movement towards a blue bioeconomy. However, several challenges need to be solved for that to happen.

To realise the promising potential of the Norwegian seaweed industry, technological solutions are essential for reducing production costs and ensuring consistent biomass quality and yield. Although the general market demand for seaweed is rising in the Western world (World Bank, 2023), Norwegian seaweed aquaculture remains unprofitable on the small scale it currently operates. New engineering solutions, automatisation, and robotics technology are pointed out as key to conquering several challenges of achieving large-scale industrial seaweed production (Kim et al., 2017). Saether et al. (2024) state that the cultivation technology used in the Western world is time and resource-intensive, yielding low production volumes. This is exemplified by a low degree of automation throughout the production cycle, from seedling cultivation to farm operations, monitoring, harvesting, and processing. Skjermo et al. (2014) states that large-scale production must also be predictable. To achieve this, the authors highlight the need for automated biomass monitoring during the sea-based on-growing phase.

1.3 Conventional seaweed biomass monitoring and remote sensing approaches

Current industry practices for monitoring biomass and growth yield primarily depend on visual or destructive in-field (*in situ)* measurements of a small sub-section of the farm, using this as a proxy for overall conditions (Overrein et al., 2024). This labour-intensive and time-consuming approach is constrained to a small sample size that does not show a reliable picture of the entire farm, even on the small scales of today's industry (Overrein et al., 2024). A monitoring system that provides relevant and objective data for farm management and operations is crucial for transitioning towards more knowledge-driven and automated practices (Føre & Alver, 2023). This underlines the need for scalable and automated monitoring techniques to handle large-scale production without sacrificing accuracy.

To address some of the limitations of field-based monitoring, remote sensing is increasingly replacing or supplementing conventional methods in aquatic studies (Cavanaugh et al., 2021; Rowan & Kalacska, 2021). The benefits of remote sensing include its efficiency, large-scale coverage and flexibility (Ashraf et al., 2010; Free et al., 2020). In a review of remote sensing of submerged aquatic vegetation, including seaweed, Rowan & Kalacska (2021) showed that remote sensing has already been applied to determine distribution, canopy density, cover classes, health and species. The application of remote sensing for assessing biophysical properties at higher resolutions, like canopy biomass or growth rates, is yet to be extensively explored. However, there has been some research on monitoring surface-level traits that can be visually observed, such as biomass (Gao et al., 2018; Free et al., 2020). This applies to surface-canopy forming kelps that have been monitored with a variety of aerial imaging technology to document changes in canopy area and biomass for wild kelp, as well as to estimate the harvestable biomass of cultivated kelp (Cavanaugh et al., 2021).

Remotely Operated Vehicles (ROVs) and Autonomous Underwater Vehicles (AUVs) are monitoring platforms that can be used for remote sensing from the water column, which makes them suitable for collecting high-resolution data. Underwater vehicles provide easier access to aquatic environments that would traditionally have to be accessed by divers or submerged equipment. An ROV is operated from a base station on the surface, usually placed on a boat or the shoreline. The ROV is connected to the base station by a tether that transmits commands from the controls to the ROV and sends video and data back to the operator in real time. AUVs operate without direct connection to an operator, using onboard systems for navigation, power and data storage. They are capable of performing operations with varying degrees of autonomy, enabling them to execute pre-set tasks with little to no direct human involvement (Sørensen et al., 2020). ROVs and AUVs can be equipped with a variety of payload sensors (e.g., optical, acoustic, and environmental) to best suit the specific operation, using remote sensing and/or *in situ* sampling. ROVs and AUVs are commonly deployed to gather underwater imagery through optical sensors (Johnsen, Mogstad, et al., 2020). Pilot studies on optical monitoring of wild kelp distribution illustrate the use of both an AUV equipped with red-green-blue (RGB) cameras (Bewley et al., 2012) and a ROV outfitted with an underwater hyperspectral imager (Summers et al., 2022).

Stenius et al. (2022) proposed a system for autonomous seaweed farm inspection, featuring a method for monitoring biomass with an AUV outfitted with side-scan sonars. Sonar technology is effective for estimating the biomass of macroalgae species with gas-filled pneumatocysts, as they produce strong acoustic returns (Wilson, 2011). However, the two species most commonly cultivated in Norway (*S. latissima* and *A. esculenta*) lack these. Addressing this research gap is crucial for the Norwegian seaweed industry (Skjermo et al., 2014), as increased automation and monitoring frequency would provide a faster rate of knowledge for optimising growth, yield predictions and planning of farm logistics (Overrein et al., 2024).

1.4 Underwater imaging and computer vision segmentation

Recent technological advancements in aerial and satellite imaging have established these approaches as essential tools for terrestrial monitoring and management (Rowan &

Kalacska, 2021). Unfortunately, their effectiveness is significantly reduced in marine environments as there exist several additional constraints in underwater imaging (Johnsen et al., 2020). This is primarily due to the optical properties of water, which affect how light propagates through the medium. The inherent optical properties (IOPs) of water describe how light is absorbed and scattered by water molecules and suspended particles (e.g. phytoplankton, coloured dissolved organic material (cDOM), and total suspended matter (TSM) and do depend on the ambient light conditions. The apparent optical properties (AOPs) depend both on the components of the medium (the IOPs) and on the directional structure of the light. This interplay between IOPs and AOPs results in rapid light attenuation through the water column, causing a reduction in light intensity, colour absorption and blurring effects, complicating the capture of clear, accurate underwater images. The effect of the AOPs limits the range at which optical sensors can capture high-resolution data (Ludvigsen & Sørensen, 2016), necessitating a platform that positions the sensor close to the object of interest. In the case of monitoring submerged kelp with data from underwater imaging, underwater vehicles, specifically ROVs and AUVs, are frequently applied for their manoeuvring capabilities.

To obtain quantitative data from optical imaging is challenging (Ludvigsen & Sørensen, 2016), but the rapidly evolving field of computer vision (CV) has facilitated the development of numerous new methods for the automatic processing and analysis of footage from aquaculture farms (Føre & Alver, 2023). CV enables computers to interpret and understand visual information from images or videos using advanced algorithms and mathematical models. Recent advancements in artificial intelligence, especially within the sub-field of machine learning, have highlighted CV as an increasingly important field for research and development (Yan, 2023). CV can be used for extracting a broad range of quantifiable data from visual inputs, such as pattern recognition, movement tracking and object detection (Yan, 2023). Image segmentation is the foundational process behind object detection. It divides the image into distinct regions with similar characteristics such as colour, intensity, or texture. These segmented regions act as blocks of information for subsequent classification or spatial processes.

A novel advancement in object detection is the Segment Anything Model (SAM) (Kirillov et al., 2023), which leverages deep learning and state-of-the-art neural networking to address a wide array of segmentation tasks. The SAM introduces a user-guided (promptable) segmentation framework capable of handling new tasks and datasets beyond its initial training. To achieve this, the SAM has been trained on the largest segmentation dataset to date, comprising over 1 billion segmentations in 11M images. It serves as a foundation model for object-based segmentation tasks as an alternative to task-specific models made for individual contexts. However, for scenarios where the foundation model fails, the SAM framework is made to be specialised (fine-tuned) by training on task-specific images, building on top of its massive foundation. This can be useful when dealing with scenarios not well represented in the SAMs original training set, such as underwater imaging.

While the optical properties of water make underwater imaging a challenging field in computer vision research (McGlamery, 1980), recently development has transitioned several theoretical concepts into commercially applied product (Yang et al., 2020; Føre & Alver, 2023). Although this is currently mostly in fish-based aquaculture, using robotics in combination with underwater imaging has also led to several projects in seaweed aquaculture, mostly related to object detection.

1.5 *In situ* seaweed biomass monitoring using underwater imaging

In a study conducted by Bell et al. (2020) a small dataset of underwater imagery captured by an RGB camera mounted on an ROV was used to train a deep-learning segmentation model for object detection at an offshore seaweed cultivation farm. The model successfully classified kelp juveniles, tags and longlines by segmenting the observed object area. The automated analysis of underwater colour imagery through machine-learning models shows potential for frequent monitoring of juvenile kelp on offshore farms. Even though the study focused on object classification, its success in segmenting the pixel area of kelp juvenile illustrates the potential of using CV and deep-learning models for structural metric estimations. The spatial calibration of pixel area to metric area has been frequently used for area estimations from remote sensing imagery. Jin et al. (2023) used object-based segmentation to identify seaweed farms areal extent and spatial distribution. However, very little research has been done on area estimations from segmented underwater imaging of cultivated kelp.

Gerlo et al. (2023) proposed a method for monitoring the growth of cultivated *S. latissima* canopies by deriving area estimations from underwater RGB stereo imaging. The canopy area from side view images was annotated and used to train a deep-learning model to automate the task. The model demonstrated high precision in segmenting the canopy coverage, achieving an Intersection over Union (IoU) of 90% to the manual annotations. The stereo imaging allowed for triangulation techniques to estimate the distance from the camera to the canopy, facilitating the conversion of pixel area into square meters. These underwater images were captured from a boat using a submerged camera setup, marking a preliminary step toward applying similar image processing techniques from an underwater vehicle. Overrein et al. (2024) used a mini-ROV to capture RGB images of kelp canopies to derive canopy area estimations and evaluate its viability as a proxy for biomass. The authors used conventional segmentation techniques, such as shift clustering, colour segmentation and adaptive thresholding, to calculate canopy pixel area and converted it to square meters using a scale bar. Their correlation analysis showed a strong relationship between the area estimations and its corresponding field-measured biomass ($r^2 = 0.95$), indicating that canopy area can be a robust proxy for biomass.

1.6 Aims of this study

The primary aim of this study was to investigate *in situ* biomass monitoring of cultivated kelp using underwater RGB imaging and the SAM, a state-of-the-art foundation model for image segmentation. For this purpose, we employed a mini-ROV to image side and top-down views of the cultivation line. The SAM was used to derive the pixel area of small canopy sections, which was spatially calibrated to area estimations and correlated with field-measured biomass.

In support of this aim, the study focused on the following objectives:

1. Compare the relationship between canopy area estimations from side and top-down views and field-measured biomass with conventional biomass estimations.
2. Evaluate and quantify the impact of measured IOPs, specifically Chl *a* and turbidity, on image quality and observed accuracy of the SAM-derived segmentations.
3. Compare the performance of the SAM against conventional segmentation techniques used by Overrein et al. (2024), focusing on observed segmentation accuracy and ease of use.

2 Material and methods

2.1 Study area and sampling methods

The fieldwork for this study was carried out at the seaweed cultivation farm Måsskjæra, owned by Seaweed Solution (SES) and located on the island of Frøya, on the outer coast of Trøndelag, mid-Norway (Figure 2.1a). The island of Frøya is considered a marine biological hotspot due to its shallow, irregular bathymetry and significant water mixing, resulting in high primary production and biological diversity (Fragoso et al., 2021). The hydrography of the region is predominantly influenced by two major currents: the brackish-influenced Norwegian Coastal Current (NCC) and the saline and nutrient-rich Norwegian Atlantic Current (NAC) (Skagseth et al., 2011). The NCC transports low salinity water northwards along the Norwegian coast, accumulating freshwater from local runoffs along the way (Skagseth et al., 2011). Beneath NCC, the NAC usually flows, but during spring and summer, occasional upwelling of its warm and nutrient-rich water occur (Skagseth et al., 2011). This dynamic interplay between the currents contributes to making the area optimal for both wild harvest and aquaculture activities, as evidenced by previous research (Tiller et al., 2015; Ervik et al., 2018).

Data collection was conducted six days at intervals of 2 to 4 weeks from March to June 2023, consistent with the growth period of *S. latissima* in spring (Førde et al., 2016). The sampling dates were chosen to assess whether the proposed biomass estimation is suitable across a variety of environmental conditions (e.g. before the phytoplankton spring bloom versus during the bloom) and seaweed growth densities (e.g. from sporophyte juveniles to “bushy” canopies).

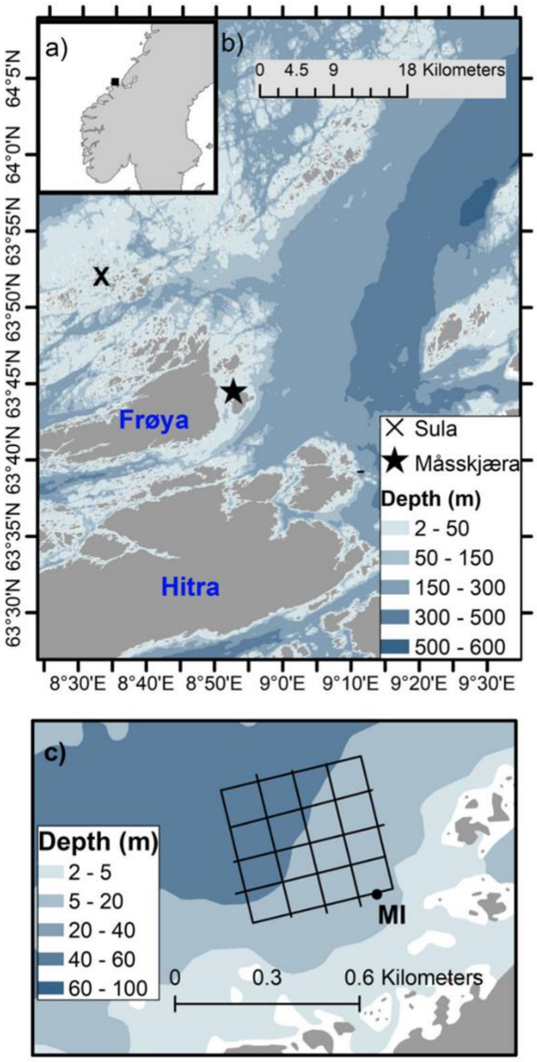

Figure 2.1: Map of a) mid-Norway showing the location of Frøya at the coast of Trøndelag (square) and b) the island of Frøya with the location of Måsskjæra seaweed cultivation farm (star) and Sula meteorological station (collection of wind data) (cross). Lastly, an illustration c) of Måsskjæra seaweed cultivation farm and the collection site Måskjæra Inside (MI). Illustration by Overrein et al. (2024).

Due to the exposed location of the fieldwork, data sampling was constrained to days with weak wind speed (< 10 m s^{-1}) to ensure safe working conditions. Image sampling was timed to coincide with slack tide, the short time period with still water between changing tides, aiming for the most vertical orientation of *S. latissima*. However, due to logistical challenges with weather and boat availability, imaging surveys also occurred in other tidal conditions (Table 2.1)

Table 2.1: Overview of field day number, date, time of ROV transect, tidal level (cm), average and maximum wind speed (Sula meteorological station) and cloud coverage (Ørland meteorological station) for all sampling days at Måsskjæra seaweed cultivation farm.

Field day	Date	ROV transect (UTC+2)	Tide (cm)	Wind strength (m s $^{-1}$) (maximum)	Weather
1	16.03.23	10:20 - 10:50	108-100 (Low)	6.8 (8.4)	Sunny
2	29.03.23	10:00 - 10:30	114-106 (Low)	5.4 (7.9)	Sunny
3	18.04.23	08:00 - 08:30	119-143 (Rising)	7.9 (9.5)	Partially sunny
4	25.04.23	08:20 - 08:50	78-69 (Low)	1.7 (2.6)	Cloudy
5	23.05.23	14:30 - 15:00	207-208 (High)	3.7 (5.3)	Cloudy
6	08.06.23	07:30 - 08:00	70-52 Receding)	5.4 (8.3)	Cloudy

2.1.1 Imaging survey

The mini-ROV BlueyeX3 (Blueye Robotics AS, Trondheim, Norway) was employed as a mobile sensor platform and a camera for underwater imaging (Figure 2.2). The ROV's built-in RGB camera captures imagery in Full High-Definition spatial resolution (1920 x 1080 pixels) at 25~30 frames per second, featuring a 115-degree field of view and tilt capabilities of 30° up and down. Additionally, the ROV was outfitted with a vertically mounted external camera with the same spatial resolution to capture top-down images. The design of the ROV prioritises user-friendliness, featuring an intuitive "plug and play" mobile application that facilitates individual operation through an Xbox controller interface. This system connects to the ROV via a tethered base station. When deployed from a vessel in field conditions, its compact design and automated positioning system make it well-suited for manoeuvring between the cultivation lines, ensuring operational effectiveness even in challenging environmental conditions (e.g. strong tidal currents and low water visibility).

Figure 2.2: The mini-ROV BlueyeX3 and its top-down facing external camera (and unused light source) together with its base station.

Large plastic strips were attached to the cultivation line before the image survey to outline three 1-m replicates of the kelp canopy along the cultivated line (herein referred to as canopy replicates). In addition to the strips, floaters (~ 5 cm diameter) were added because of previous challenges related to detecting the outline of the canopy replicate in the images, since the canopies "bushiness" at the later stages of the cultivation can envelop the strips (Overrein et al., 2024). In our image analysis, the 1-m distance between the floaters served as a size reference for spatial calibration of the segmented pixel area.

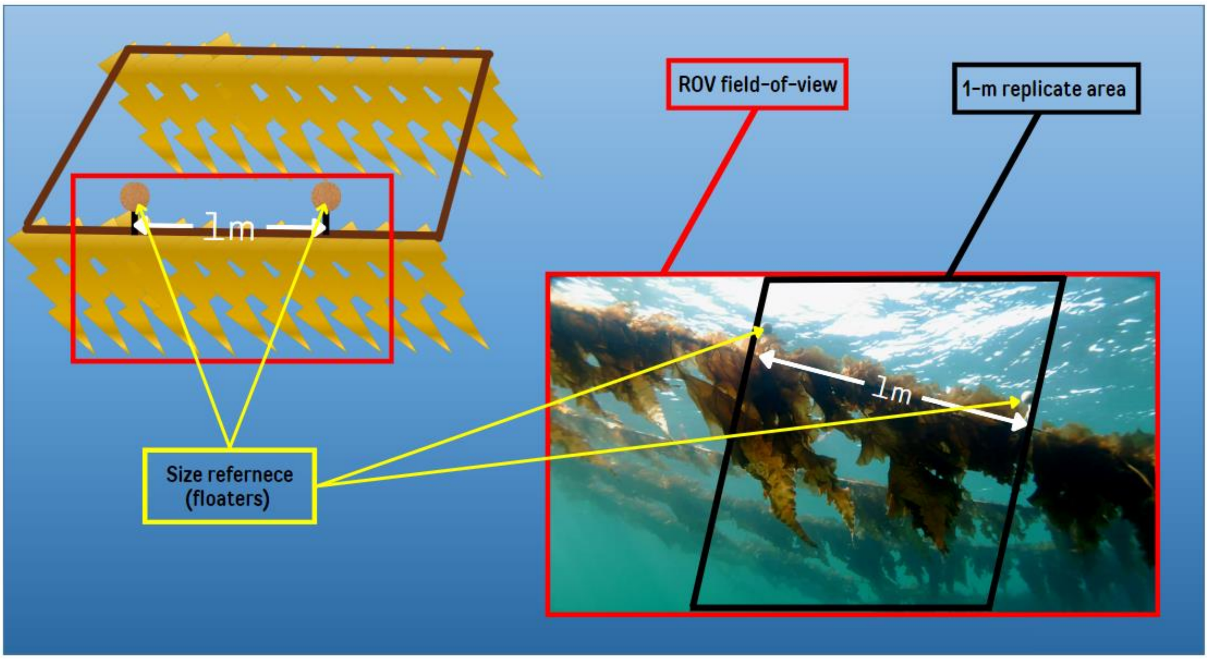

Figure 2.3: Illustration of a canopy replicate outlined with floaters as a size reference, corresponding with an *in situ* ROV image showing both field-of-view and canopy replicate area.

After outlining the canopy replicates, the ROV was deployed from a small vessel near the collection site MI and manoeuvred towards the selected cultivation line with the three canopy replicates. Given the varying conditions in currents and water visibility, trial runs were initially conducted to adjust the ROV thrust settings for optimal manoeuvrability. The ROV was navigated along the cultivation line with the internal camera pointed towards the kelp canopies hanging vertically from the cultivation line (Figure 2.4a) to capture the canopy replicates length (side view). Following this, the ROV was driven straight above the cultivation line with the external camera pointing downwards to capture the same canopy's depth (top-down view) (Figure 2.4 b)

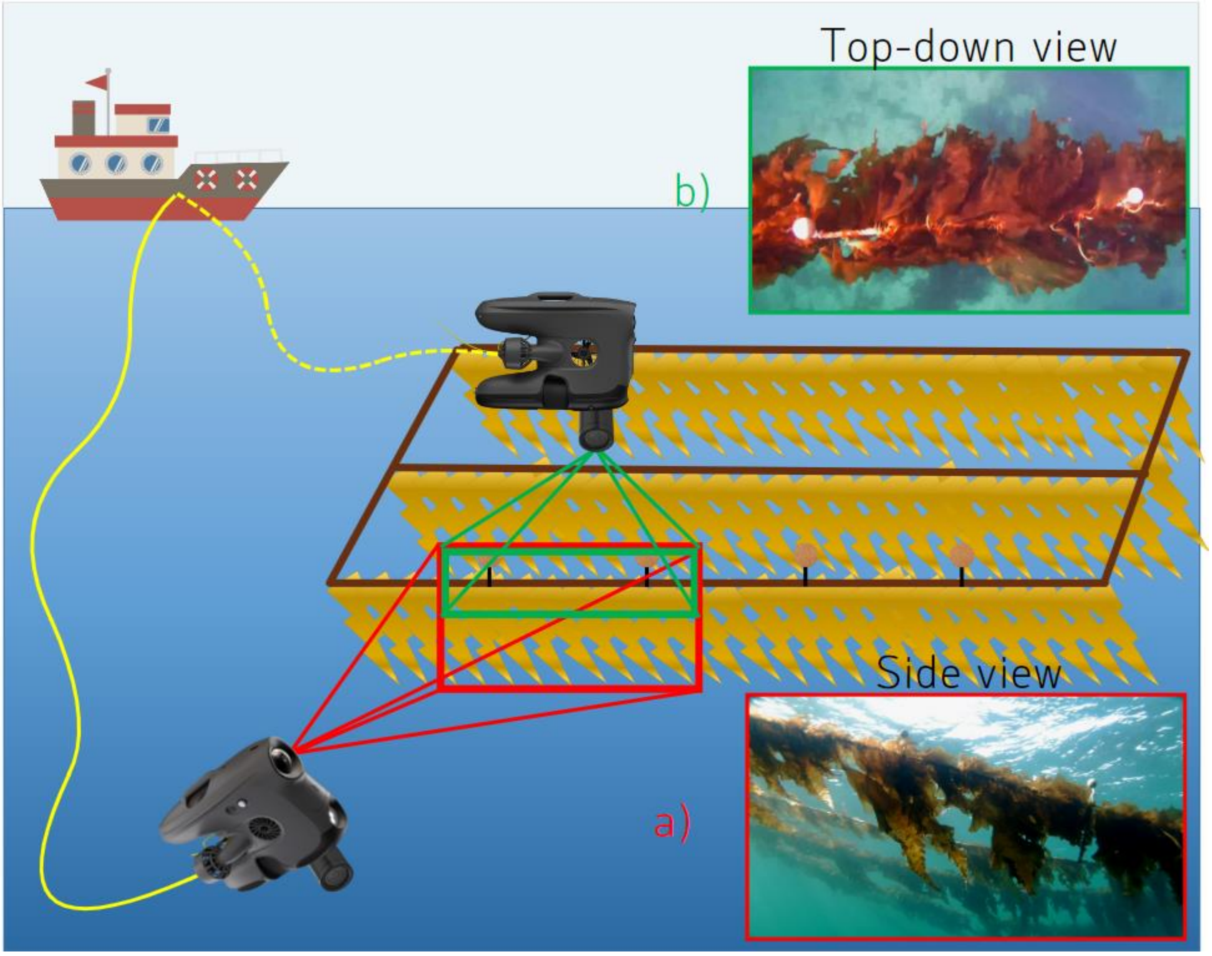

Figure 2.4: Simplified illustration of how imaging surveys of the kelp canopy replicates were conducted with ROV-transects capturing a) side view video and b) top-down view video.

2.1.2 Field-based measurements

Following each imaging survey, the three canopy replicates were harvested by hand for immediate field-based measurements. Each canopy replicate was harvested and weighed to derive wet-weight biomass per meter. Following this, all sporophytes over 15 cm from each canopy replicate were counted and sorted by their lamina length – from the tip of the lamina to the beginning of the holdfast (Figure 2.5a). For field-based length measurements, 10 sporophytes were selected from the sorted individuals to represent the population size (Figure 2.5b). These 10 individuals from each canopy replica were then measured for laminal length and maximum lamina width (Figure 2.5).

Field measurements	Description
Biomass (kg m^{-1})	Wet weight of replicate meter
Density (individuals m^{-1})	Number of individuals per replicate meter
Lamina length (cm)	Average of individiual lamina length (n=10)
Lamina width (cm)	Average of individual maximum lamina width (n=10)

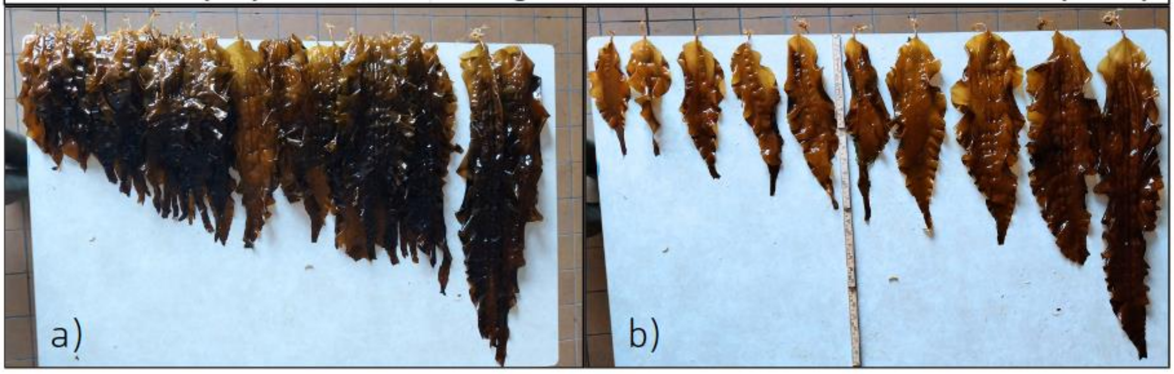

Figure 2.5: Overview of the various field measurements and examples of a) a harvested and sorted canopy replicate and b) 10 selected individuals for length measurements.

2.1.3 Environmental variables

To establish a foundation for evaluating the effects of water visibility on image quality and segmentation accuracy, a submersible fluorescence sensor (C3, Turner Designs, USA) was connected to the frame rope at station MI at a depth of ~3 meters, corresponding to the depth of the *S. latissima* canopies on the cultivation line. The sensor measured chlorophyll *a* fluorescence (calibrated to [*Chl a*] in mg m^{-3}) as a proxy for phytoplankton biomass, turbidity (Relative Fluorescence Unit, calibrated to Formazin Turbidity Unit (FTU)) for suspended particle concentration, and temperature (°C). Data measurements occurred at a 10-minute interval from mid-February to mid-June to capture the varying water conditions throughout the sampling period. Furthermore, wind speed (average hourly interval in meters per second from the same time period) was acquired from the Sula meteorological station (https://seklima.met.no/), located west of Frøya (Figure 2.1b).

2.2 Image extraction

The initial step for image extraction involved using basic video editing software, in this case Shotcut (Version 23.12; Meltytech LLC, 2024), to remove irrelevant footage from the full video recordings. With the relevant video segments isolated (the ones that contain frames of the canopy replicates), one frame (image) per second is extracted from the footage. From these images, three images per canopy replicate were selected for side and top-down views (Figure 2.6)

The selection criteria ensured that the images:

- Displayed the markers for outlining the replicate and size referencing.
- Captured the full length and width of the canopy replicate.
- Featured a perpendicular view of the kelp to minimise perspective distortion.
- Cantered the replicate within the image to reduce distortion from the camera's dome.
- Were distinct from one another to provide perspective diversity within the replicate.

This procedure generated 18 images for each sampling day (3 × 3 × 2: 3 images of the 3 canopy replicates and their 2 canopy views), cumulatively resulting in a dataset of 108 canopy replicate images (18 images × 6 sampling days). The images in the dataset were systematically labelled for subsequent image analysis; indicating the field day on which they were captured, the specific replicate meter and its canopy view.

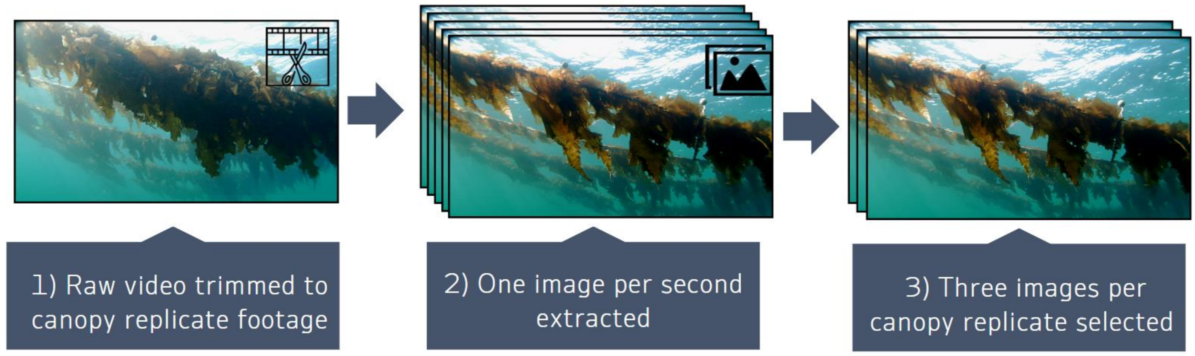

Figure 2.6: Pipeline of the process from unedited ROV-video to 1) isolated transects comprising frames of the canopy replicate, to 2) extraction of 1 frame s^{-1} and finally 3) the selection of 3 frames for further processing.

2.3 Image analysis

2.3.1 Segmentation and area estimation

The canopy replicate pixel area was segmented using OpenCV's open-source annotation tool Computer Vision Annotation Tool (CVAT). The CVAT provided a user interface for the SAM, facilitating semi-automatic and promptable segmentation (Figure 2.7). When inputting an image, the image encoder automatically generates an image embedding while the prompt encoder embeds user-provided prompts in the format of positive and negative clicks (kelp canopy or not kelp canopy). The two are combined in a lightweight mask decoder that iteratively predicts the segmentation coverage with each added prompt until a satisfactory segmentation is provided. This allowed for efficient corrections in cases where the initial canopy segmentation was inaccurate. As the SAM does not differentiate between the specific canopy replicate area and the observed canopy in general, its segmentation also covers parts of the canopy outside the defined 1-m markers.

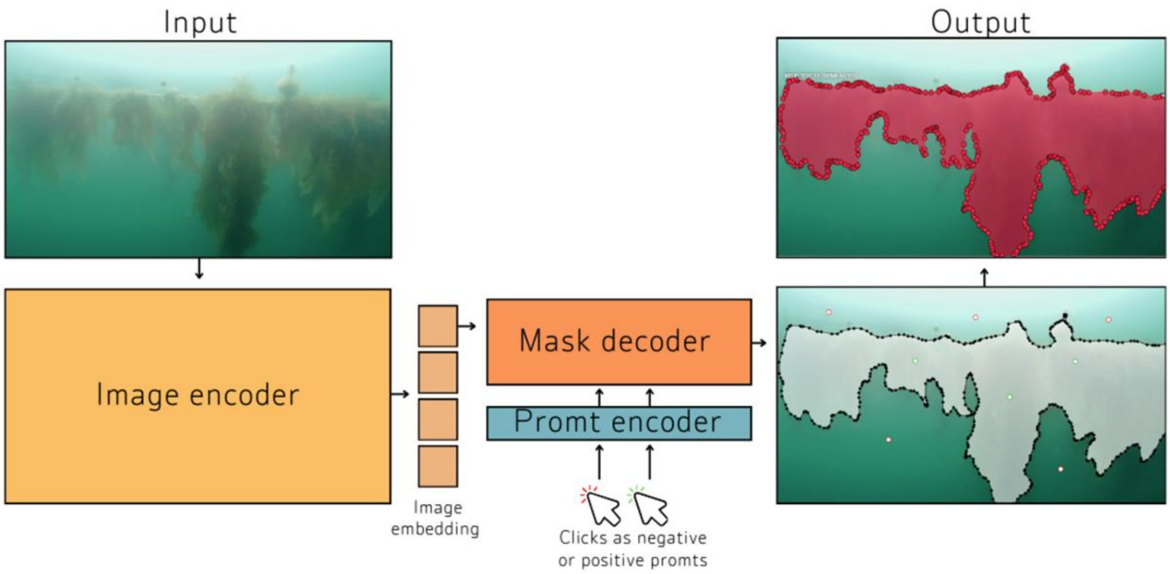

Figure 2.7: Simplified overview of how the Segment Anything model (SAM) is applied to segment the observed kelp area. The image encoder outputs an image embedding that can be adjusted by various user-provided prompts (in this case clicks) to produce segmentation masks at close to real-time speed. Illustration adapted from Kirillov et al. (2023).

When the canopy pixel area was accurately covered in the segmentation, a slicing tool available from the CVAT interface was used to remove the parts of the segmentation that were outside of the outlined canopy replicate (Figure 2.8). A polyline was drawn in the image between the two outlining floaters, serving as a size reference for spatial calibration. The output of the annotations was exported from CVAT and converted to a CSV file for processing. The CSV was processed in a script to spatially calibrate each segmentations pixel area to area in dm^2 m^{-1} using its corresponding scale bar, resulting in canopy replicate area estimations from a side and top-down view (herein referred to as canopy area estimations from side view/top-down view images).

The canopy area estimations from side view imaging represent the width and length of the canopy replicates (dm^2). To estimate the replicate's average depth (dm), the area of the top-down images was divided by the constant replicate length of 1 meter. As a proxy for canopy replicate volume (dm^3), the side view area estimations were multiplied by their corresponding average depth.

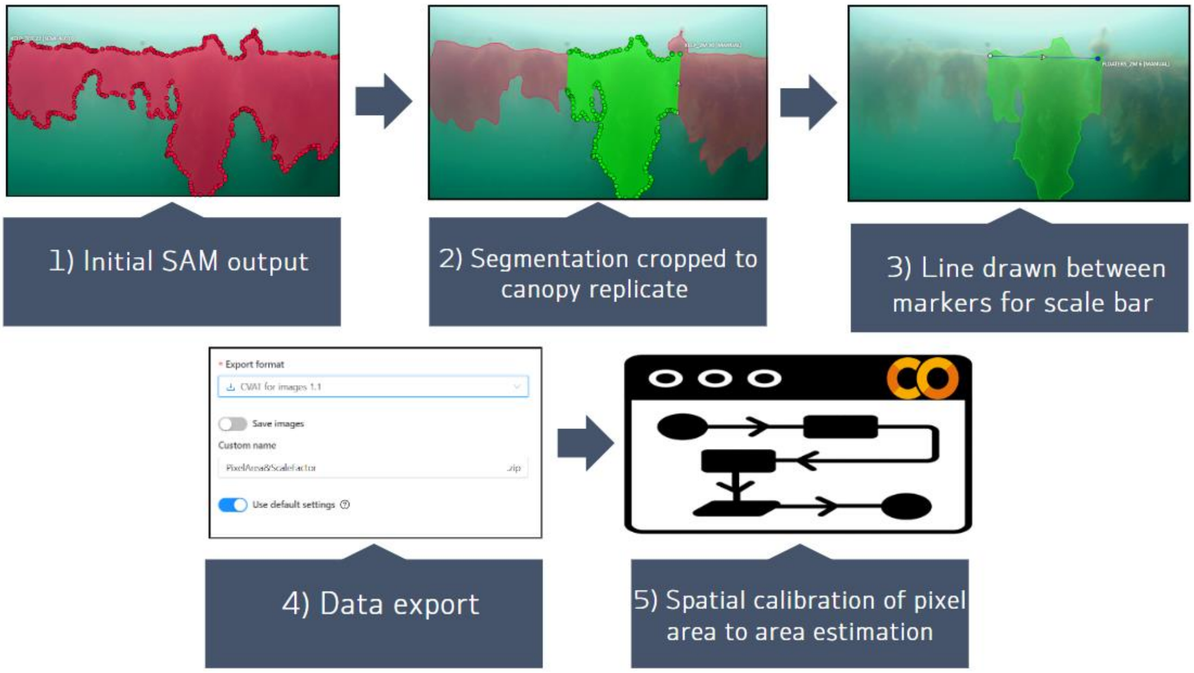

Figure 2.8: Pipeline of the cropping initial output of the Segment Anything Model (SAM) derived segmentations (Figure 2.7) and subsequent pixel area conversion to canopy area estimation in dm^2 m^{-1}

2.3.2 Image quality evaluation

As a subjective evaluation of the impact of measured IOPs, specifically [*Chl a*] (a proxy for phytoplankton biomass) and turbidity (suspended particle concentrations), on image colour and sharpness during the study period, the observed image quality for each field day was considered. To supplement this with quantitative measurements, an imaging metric analysis (Figure 2.9) was performed using the image dataset toolkit Encord Active (Version 0.1.84; Encord, 2023). The canopy replicates side view images from all field days were imported and processed using the Encord Actives library of preset image metric calculations (Green Values, Blue Values, Sharpness, and Blur), proving standardised scores for each category across all images. Sharpness and Blur have a perfect negative correlation, but were both included for illustrative purposes.

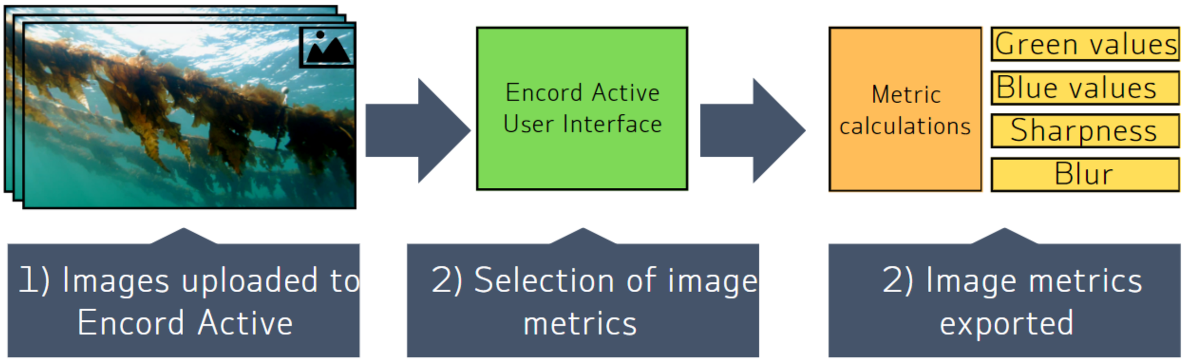

Figure 2.9: Pipeline illustrating how the side view images from all field days were imported and processed using Encord Actives library of preset image metric calculations to provide standardised scores for each category across all images.

2.4 Method comparison of segmentation accuracy and viability

Our method for deriving canopy area estimations using the SAM builds on the approach developed by Overrein et al. (2024). Their sampling method shared the same study area, field measurements, object of interest (1-m replicates of cultivated *S. latissimia* canopies), temporal range and side view perspective. Their study employed conventional segmentation techniques to derive canopy area estimations and we evaluated the SAMs performance by processing their dataset of 54 side view images (6 images × 1 canopy replicate × 7 sampling days). The observed segmentation accuracy was visually evaluated and the relationship between both canopy areal estimations and field-measured biomass was compared.

2.5 Statistical analyses

To investigate the relationships between the image quality metrics (Green Value, Blue Value, Sharpness and Blur), a principal component analysis (PCA) was conducted using the PRIMER-e software (Version 7; Clarke & Gorley, 2014). This multivariate statistical technique was used to identify the key components explaining the most variance in image colour and sharpness during the study period. The PCA was performed on standardised data to ensure that each metric contributed equally to the analysis. The results were visualised in a biplot, introducing bubbles representing [*Chl a*] on top of the PCA to discern the associations between the key image metrics and the field days corresponding [*Chl a*] nightly average (from 00:00 to 07:00).

The effectiveness of using canopy area estimations and our canopy volume proxy as indicators for field-measured biomass was investigated through power regression analyses. The regressions were performed and visualised using Microsoft Excel (Version 2403; Microsoft, 2024), with correlations plotted on a log-log scale to linearise the relationship for easier interpretation. The strength of the relationships was determined by the coefficient of determination (r^2). The same approach was used to examine the relationship between field-measured lamina length and field-measured biomass, providing a comparison for the fit of manually field-measured as a proxy for biomass.

3 Results

3.1 Environmental variables

The daily average wind speed varied greatly throughout the sampling season from ~1.5 m s^{-1} to multiple peaks above 12 m s^{-1}, reflecting the fluctuating weather patterns in the Frøya region (Figure 3.1a). Due to operational restrictions during such peaks, the average wind speed on sample days varied from 1.8 m s^{-1} (April 18th) to 7.6 m s^{-1} (March 16th).

Chl a and turbidity showed varying concentrations throughout the field period with occasional peaks. After relatively low [*Chl a*] (~0.4 mg m^{-3}) from mid-February to March, a major peak was observed at the beginning of April (up to 5.5 mg m^{-3}). After the peak, [*Chl a*] levels fluctuated between 1.0 mg m^{-3} and 2.8 mg m^{-3} throughout the rest of the field season. Turbidity followed a similar trend throughout the sampling period, with the exception of two independent peaks, one short in early March (> 0.2 FTU) and one long in mid-to-late June (> 0.2 FTU) (Figure 3.1b).

Seawater temperature maintained a stable level between 5°C and 6°C until the beginning of April before a gradual increase up to ~11.5°C at the end of June (Figure 3.1c).

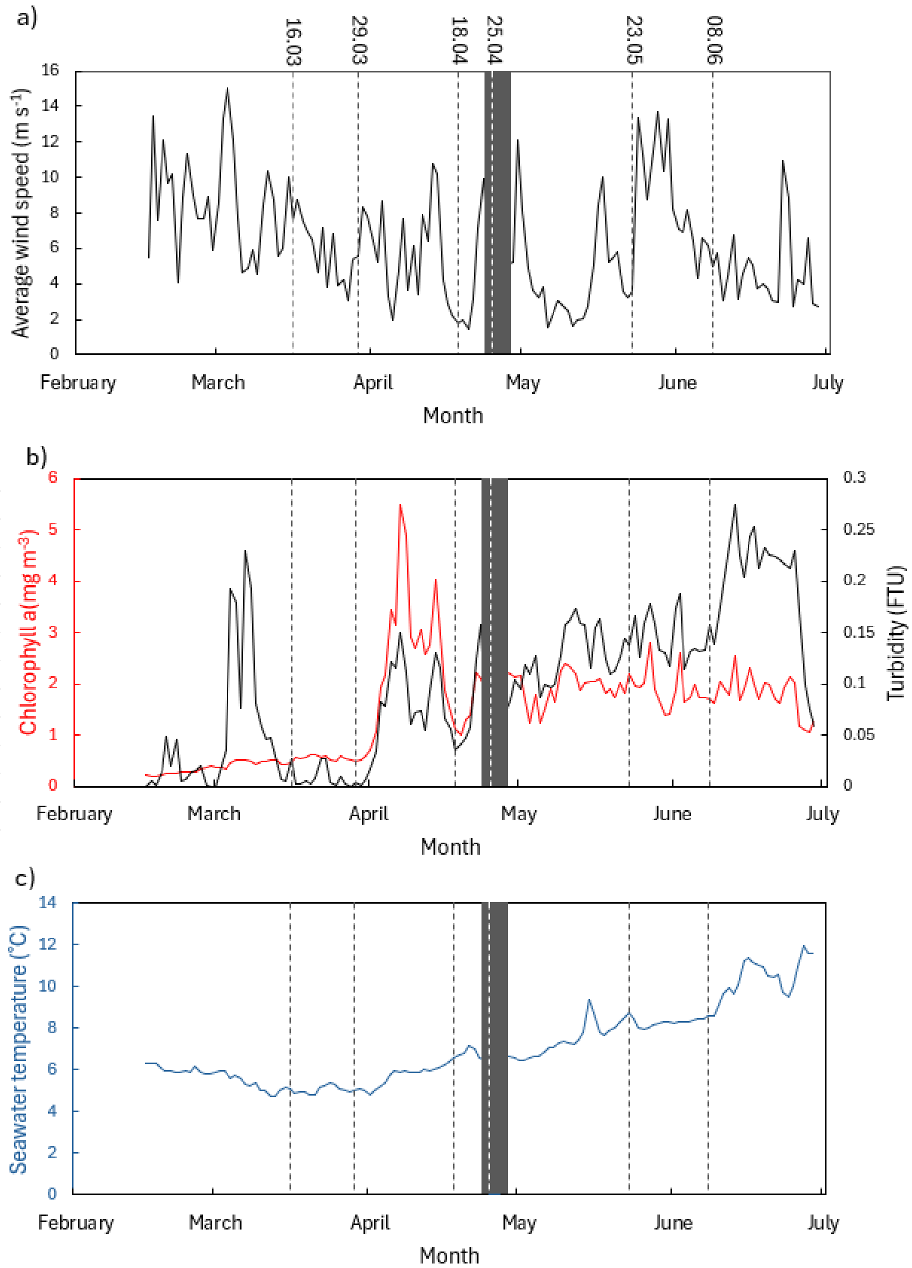

Figure 3.1: The environmental variables from mid-February to late-June 2023 with vertical lines marking each field day. The grey column represents sensor downtime. A) Average wind speed (m s^{-1}) was measured at Sula meteorological station, while B) [Chl a] (mg m^{-3}) (red), turbidity (FTU) (black), and C) seawater temperature (°C) was measured at Måsskjæra seaweed farm.

3.1.1 Observed image quality

When evaluating the image dataset used for canopy area estimations, differences in the image quality among sampling days were observed. High image quality, indicating high water visibility, was observed at the beginning of the season (March 16th and March 29th). From April 18th, the canopy sharpness was reduced, but the image quality was still good enough to outline the canopy replicate (Fig. 3.2). In the later part of the season, specifically April 25th, May 23rd, and June 08th, the image quality was consistently low, with all images displaying a distinct green hue and reduced sharpness. This indicates a significant decrease in water visibility compared to the beginning of the season.

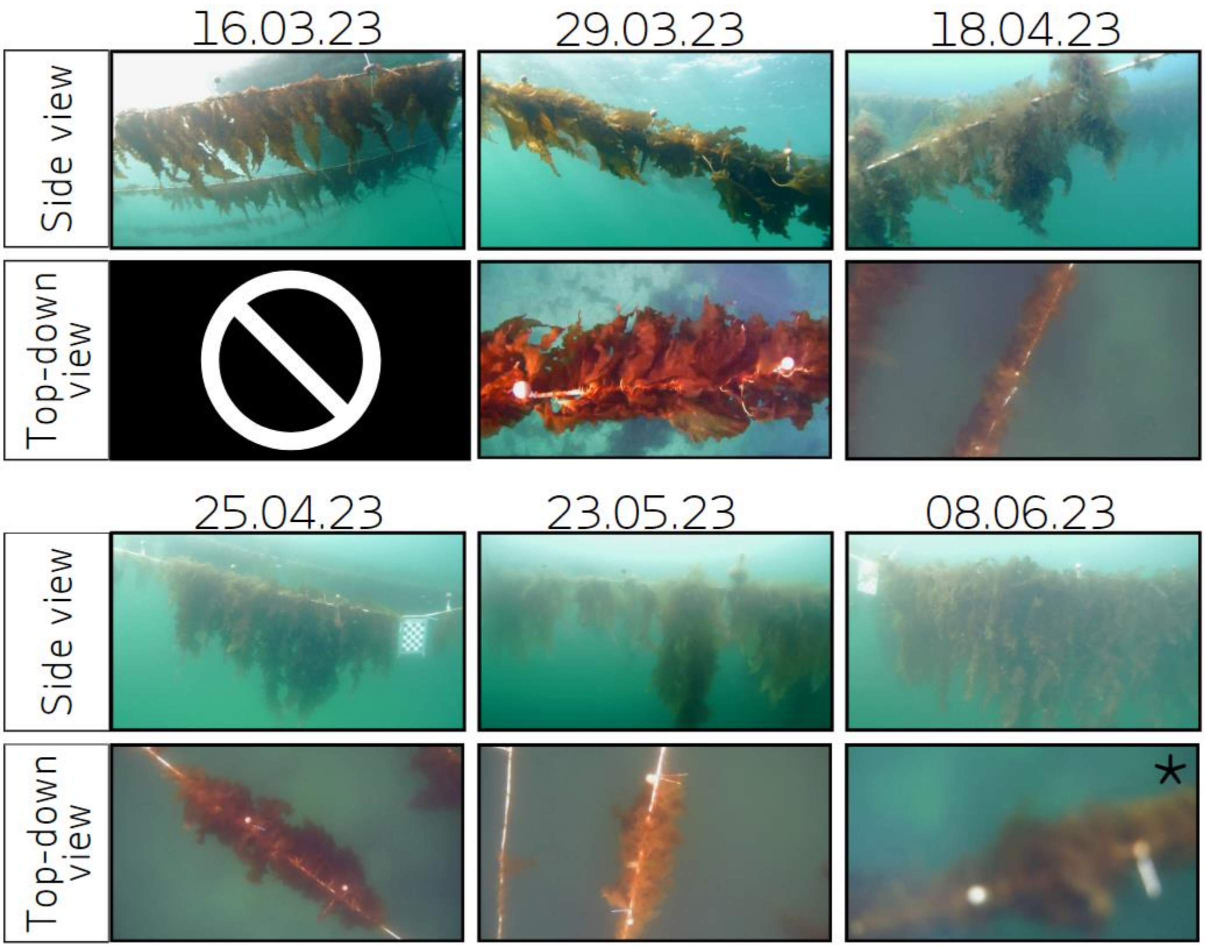

Figure 3.2: Examples of side view and top-down view images collected each day to illustrate the change in observed image quality throughout the field season. *The distinct blur in the top-down image from 08.06 is related to a camera malfunction, not water visibility.

3.1.2 Image quality metrics

The side view images of the canopy replicates showed distinct groupings of image metrics scores from the same field day, indicating consistent image quality within dates but variability across the study period. The x-axis (PC1) represents the component explaining 67.7% and a cumulative proportion of 100% together with the two additional PC axes (Table 3.1).

Table 3.1: List of the factors comprising the principal component analysis (PCA) illustrated in Figure 3.3

Axis	PC1	PC2	PC3
Eigenvalues	2130.00	699.00	320.00
Proportion of variance (%)	67.70	22.20	10.20
Cumulative proportion (%)	67.70	89.80	100.00
Variables			
Green Values	0.121	-0.993	0.001
Blue Values	0.422	0.051	-0.905
Sharpness	0.635	0.078	0.301
Blur	-0.635	-0.078	-0.301

Sharpness and Blue Values are strongly aligned with PC1. As the inverse of Sharpness, Blur correlates negatively with PC1. The images show a chronological trend, with images from early in the season scoring highest in Sharpness, with an increase in Blur and decrease in Sharpness and Blue Values as the season progressed (Figure 3.3). This corresponded with the increase in [*Chl a*] and turbidity during the same period. Images from March 16th and 29th have especially high Sharpness and Blue Values, while images from April 25th, May 23rd and June 8th showed consistently low levels.

The second axis (PC2) showed variations in Green Value, which were highest on May 23rd. The bubble symbols representing [*Chl a*] illustrate this trend, with high Green Values corresponding to high [*Chl a*].

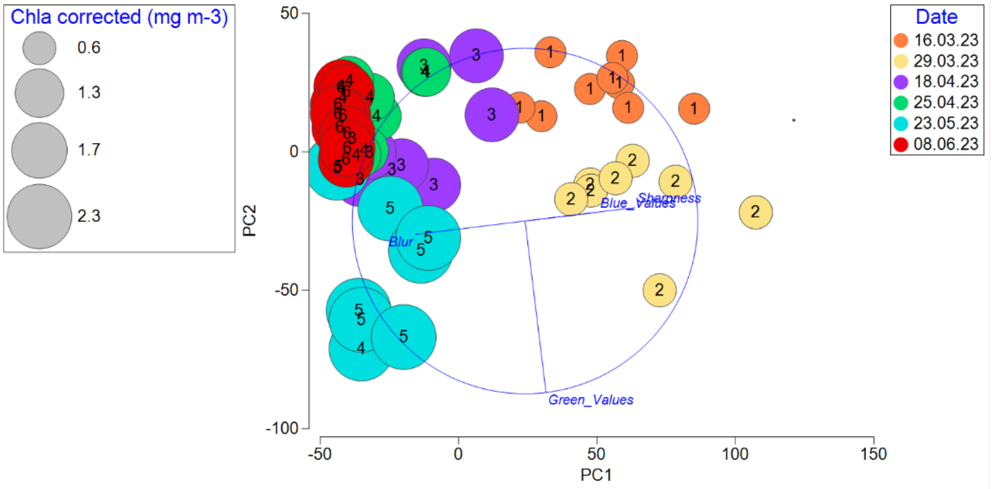

Figure 3.3: Principal component analysis (PCA) illustrating the key components explaining the most variance in image quality for canopy side view images throughout the field season. The temporal increase in Blur corresponds to the increased [*Chl a*] and turbidity during the study period.

3.2 Lamina-length correlated to field-measured biomass

The field-measured biomass from the canopy replicates ranged from 0.78 kg m^{-1} to 6.60 kg $m^{-1,}$ with a general trend of increasing biomass as the season progressed. A similar trend is seen in the field-measured lamina length, with an average lamina ranging from 36.8 cm to 89.2 cm (standard deviation ranging from 11.2 cm to 32.8 cm). The correlation of field-measured lamina length and biomass demonstrated a positive power relationship (r^2=0.622, $p<0.01$, Figure 3.4).

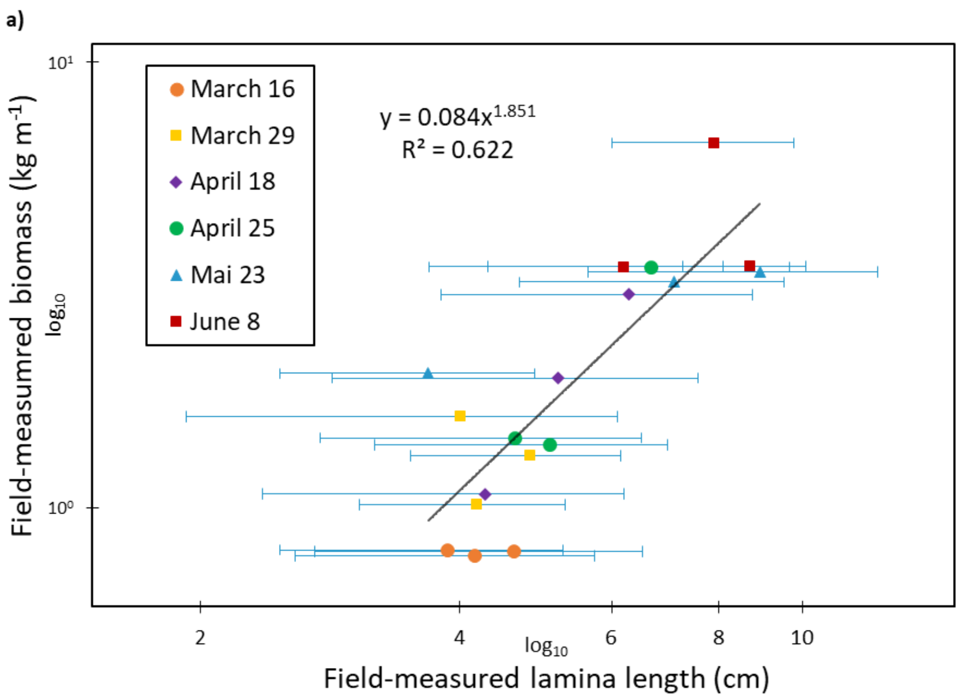

Figure 3.4: Log-log plot visualising the relationship of the field-measured average lamina length (cm) and its corresponding field-measured biomass (kg m^{-1}).

3.3 Canopy estimations correlated to field-measurements

Table 3.2 Overview of the canopy estimations and corresponding units

Canopy estimations	Description
Side view area (dm^2 m^{-1})	Segmentation pixel area converted to area
Top-down view area (dm^2 m^{-1})	Segmentation pixel area converted to area
Volume proxy (dm^3 m^{-1})	Side veiw area (dm^2) x (Top-down area / Length of Top-down area)

3.3.1 The SAM segmentation quality

In general, water visibility decreased from the beginning to the end of the season. The impact of water visibility in the SAM-derived segmentation was visually assessed by qualitatively evaluating whether the segmentation (red polygon) and size reference (blue polyline) correctly aligned with the canopy replicate (Figure 3.5).

Although images were significantly degraded towards the end of the study, displaying a distinct green hue and reduced sharpness, the segmentations still aligned well with the canopy replicates (see example in Figure 3.5).

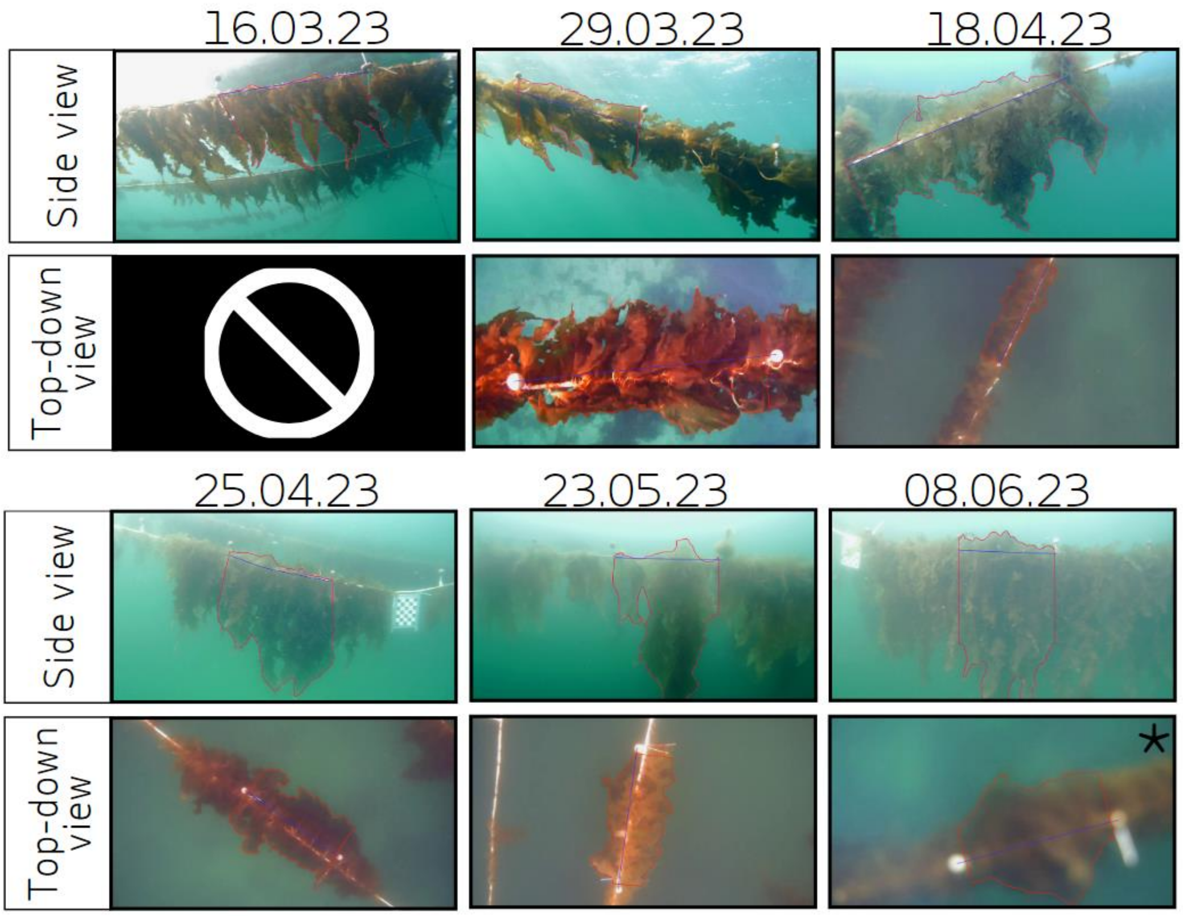

Figure 3.5: Examples of segmentations from images of side and top-down views collected to illustrate the consistently satisfactory segmentation quality throughout the study period season. *The distinct blur in the top-down image from 08.06 is related to a camera malfunction, not water visibility.

3.3.2 Canopy area estimation from side view images

Canopy area estimations from side view images ranged from 24.26 dm^2 to 141.23 dm^2 (standard deviation from 0.88 dm^2 to 11.54 dm^2). When correlating the canopy area with biomass, a strong power relationship is observed (r^2=0.769, p<0.01, Figure 3.6a)

As a comparison, the canopy area also demonstrated a positive power relationship with field-measured length (r^2=0.656, p<0.01, Figure 3.6b)

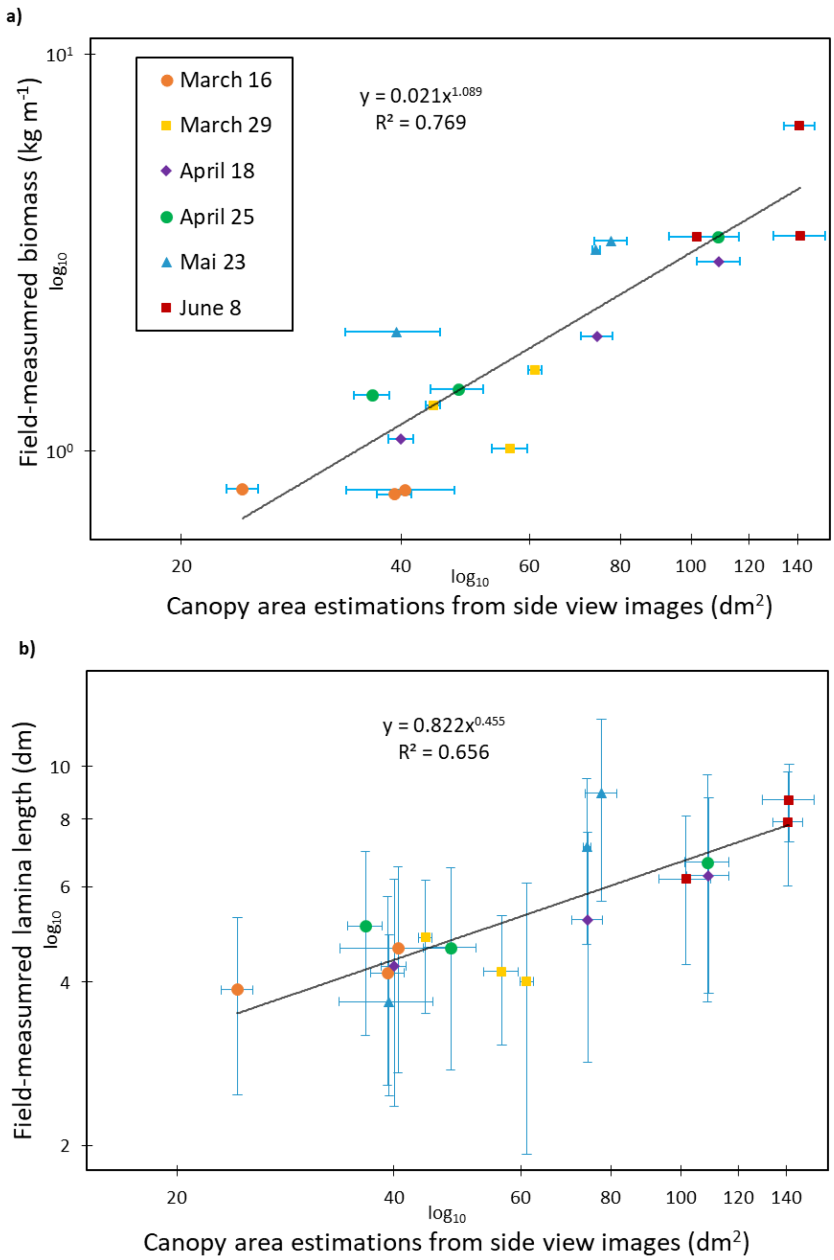

Figure 3.6: Log-log plot visualising the relationship between the canopy area estimations from side view images and its corresponding a) field-measured biomass (kg m^{-1}) and b) field-measured lamina length (dm).

3.3.3 Canopy area estimations from top-down view images

Canopy area estimations from top-down view images ranged from 19.45 dm^2 to 53.63 dm^2 (standard deviation from 0.35 dm^2 to 3.25 dm^2). There was no top-down view footage on March 16th. When correlating canopy area from top-down view images with biomass a weak power relationship is observed (r^2=0.365, p = 0.052, Figure 3.7a).

Canopy estimations from top-down view images was compared to the corresponding field-measured sporophyte density to discover a strong positive power relationship (r^2=0.676, p<0.01, Figure 3.7b)

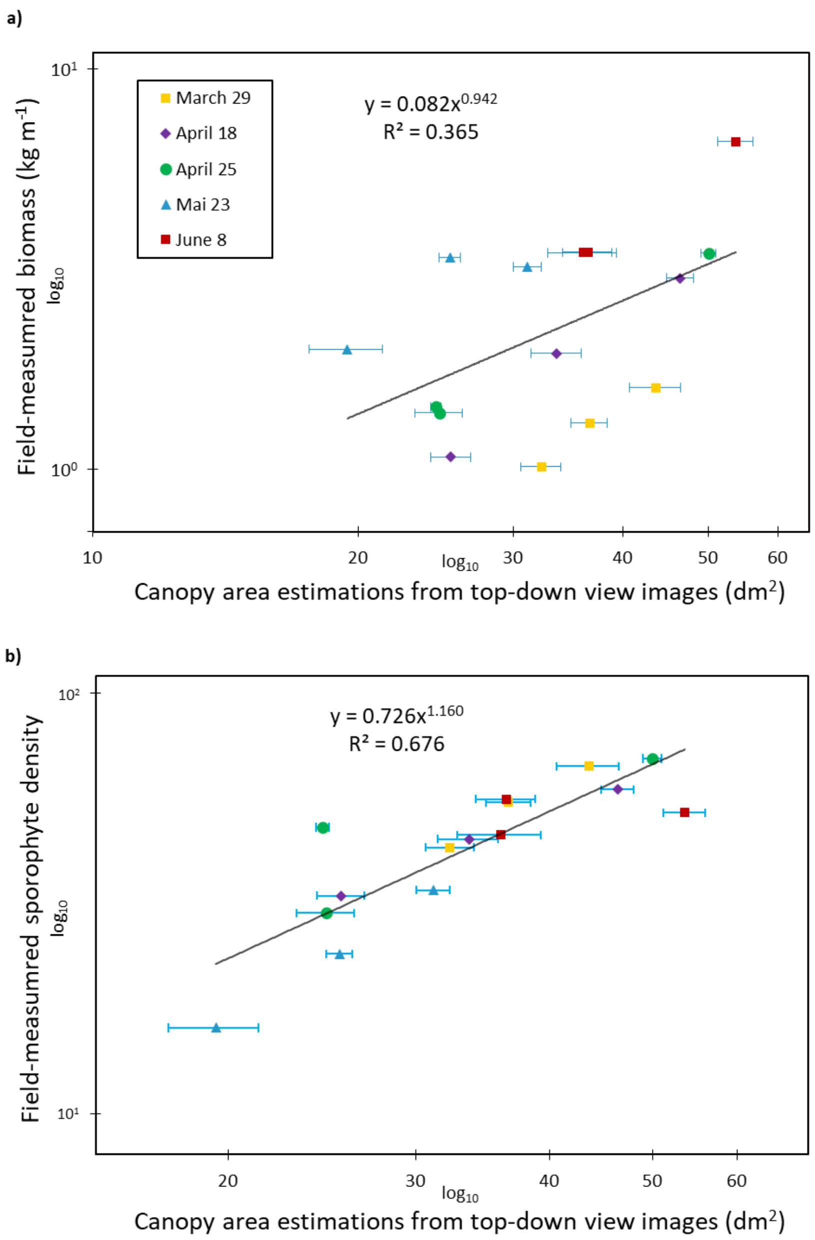

Figure 3.7: Log-log plots visualising the relationship between canopy area estimations from top-down view images and its corresponding a) field-measured biomass (kg m^{-1}) and b) field-measured sporophyte density.

3.3.4 Canopy volume proxy

The correlation analysis between the canopy volume proxy and field-measured biomass displayed a positive power relationship (r^2 = 0.681, p<0.01, Figure 3.8).

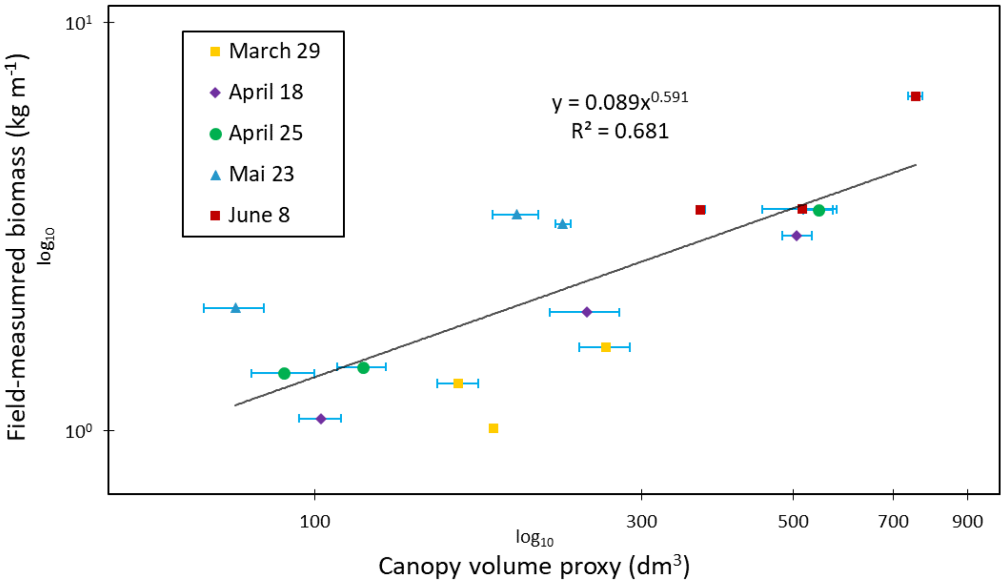

Figure 3.8: Log-log plot visualising the relationship between the canopy volume proxy and its corresponding field-measured biomass (kg m^{-1}).

3.4 Comparison of segmentation approaches for canopy area

3.4.1 Observed segmentation accuracy

In conditions with high water visibility, both the SAM and the conventional segmentation techniques implemented by Overrein et al. (2024) provided segmentations of observed high segmentation accuracy. However, during conditions of low water visibility, the conventional segmentation techniques missed substantial parts of the canopy area, while the SAM maintained a high segmentation accuracy (see examples in Figure 3.9).

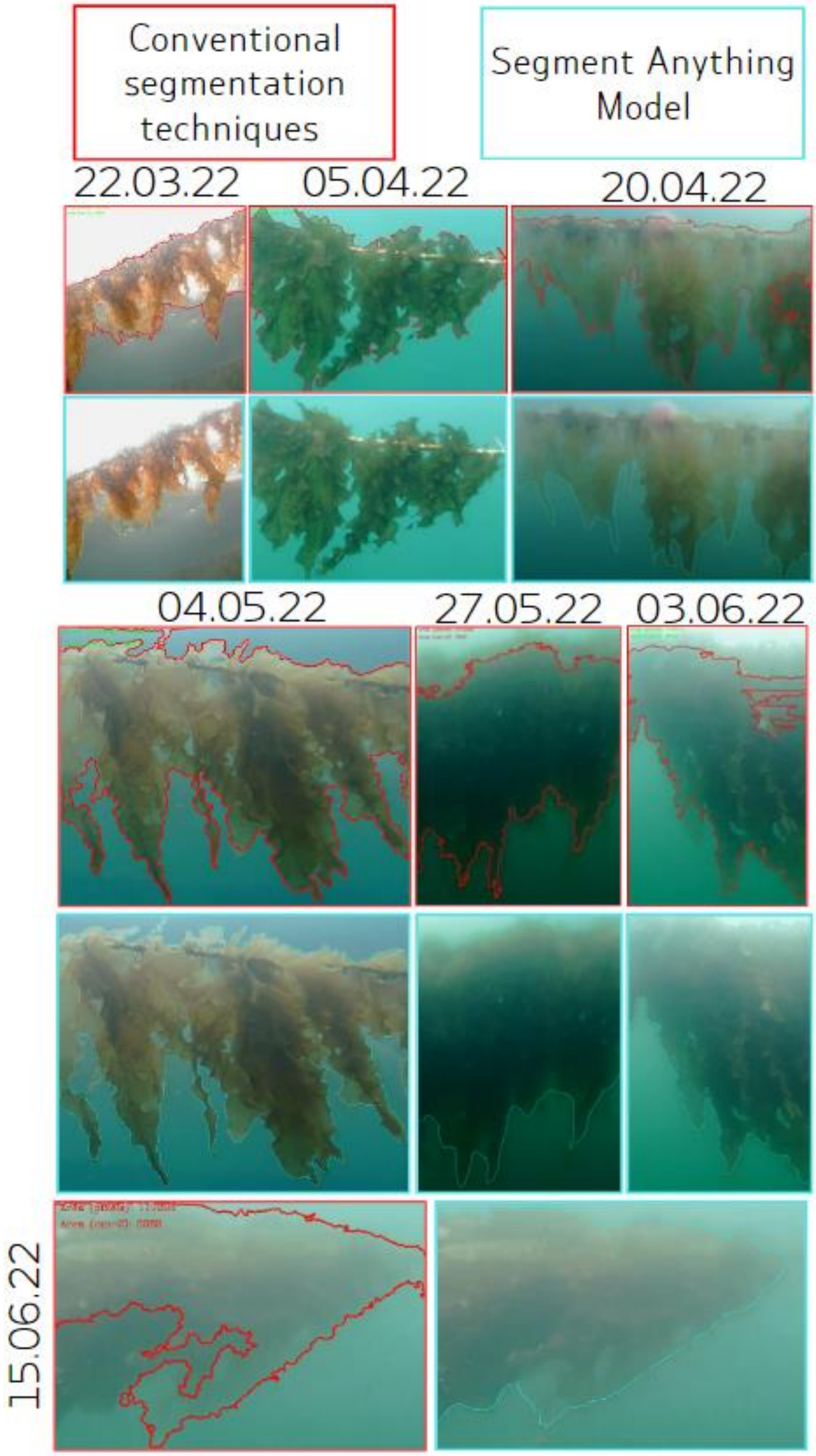

Figure 3.9: Canopy side view images segmented with the Segment Anything Model (SAM) (blue line) and the conventional segmentation techniques (red line) used by Overrein et al (2024), to illustrate the change in observed segmentation quality throughout the study period.

3.4.2 Comparison of CV-derived area estimations from different methods

The SAM-derived area estimations used in this study (Figure 3.10a) and the CV-derived area estimations from Overrein et al (2024) (Figure 3.10b) demonstrate a similarly strong power relationship to field-measured biomass, with the SAM achieving a stronger correlation(. The average standard deviation for Overrein's CV-derived area was 5.06 dm^2 (range from 2.34 dm^2 to 9.16 dm^2) while, for the SAM-derived area, it was 4.67 dm^2 (range from 1.62 dm^2 to 11.12 dm^2)

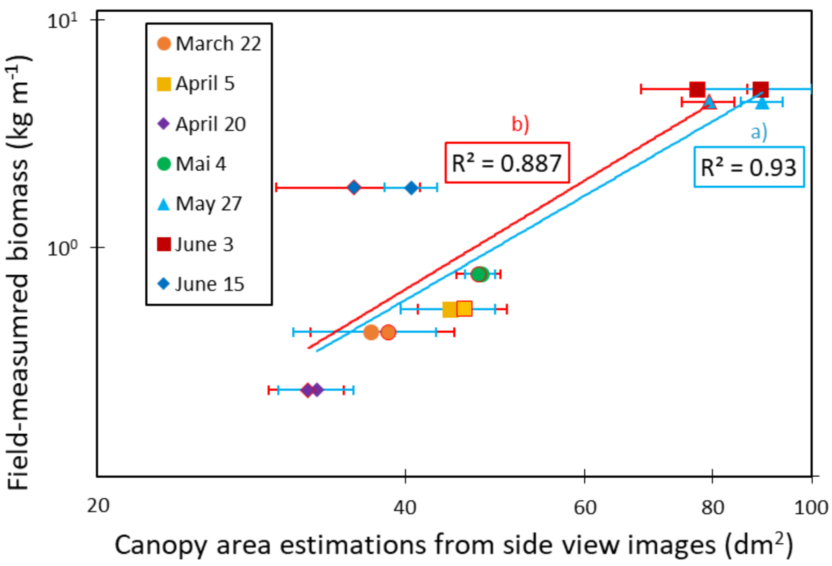

Figure 3.10: Log-log plot comparing the SAM approach for area estimations (blue) used in this study to the conventional segmentation techniques (red) used by Overrein et al. (2024) by correlating the canopy area estimations from side view images to field-measured biomass (kg m^{-1}).

4 Discussion

4.1 Kelp canopy biomass estimations from *in situ* underwater RGB imagery

Our correlation analysis showed a positive power relationship (r^2 = 0.769, n = 18) between the side view area estimations and field-measured biomass. This correlation is stronger than the one observed between manually-derived lamina length and field-measured biomass (r^2 = 0.622, n = 18), suggesting that canopy area estimations are a more robust proxy for canopy biomass than lamina length. Our findings are comparable to the strong relationship (r^2 = 0.887, n = 7) between area estimations and field-measured biomass shown by Overrein et al. (2024), where the authors used conventional segmentation techniques, such as shift clustering, colour segmentation and adaptive thresholding, to calculate pixel area. The study by Overrein et al. (2024) and this thesis demonstrate the potential of deriving structural metrics from underwater imagery for kelp canopy biomass estimations. However, both studies were done in a small sub-section of the cultivation farm, where only a few lines were assessed. Further validation through large-scale experiments is necessary to reduce the statistical uncertainty related to the relatively small sample size used in these studies. A challenge with large-scale experiments using remote sensing to asses biophysical properties (e.g. biomass and lamina length) of submerged aquatic vegetation, like *S. latissima* canopies, is the substantial amount of supplementary data needed to produce accurate results (Rowan & Kalacska, 2021). Our small-scale and preliminary monitoring study required significant work efforts to sample field-measured wet weights to validate the biomass estimations and monitor environmental variables to evaluate the effect of IOPs on segmentation quality. Despite of the challenges, the development of an automated and scalable monitoring method remains a prerequisite to achieving a cost-effective and large-scale production (Skjermo et al., 2014).

Agriculture have faced similar challenges in large-scale biomass estimations of crop canopies. Traditional methods of crop biomass measurements, which involve harvesting, drying, and weighing plant samples, are accurate but inherently destructive, labour-intensive, and time-consuming. Consequently, these traditional methods are impractical for large-scale spatial and temporal measurements (Wang et al., 2016). To address this, remote sensing applications have been extensively used due to their ability to collect scalable temporal and spatial information at a relatively low cost (Ene et al., 2018). Maimaitijiang et al. (2019) employed stereo imaging from an unmanned aerial vehicle (UAV) to create high-density point clouds of soybean canopies. Their study showed that 2D canopy structure metrics, such as mean canopy height and projected basal area, correlated well with field-measured biomass (r^2=0.801 and 0.702, respectively). However, as identified by the authors, both measurements are derivatives of one-dimensional pixel information, which tends to reach a plateau as biomass continues to increase.

The top-down view imaging of the kelp canopies has a comparable canopy view angle to aerial monitoring of projected basal area, but big differences in spatial resolution. The power relationship between the kelp canopy top-down view area and field-measured biomass was noticeably lower (r^2 = 0.365) than what has been observed for aerial above-ground biomass estimations of crop canopies (Maimaitijiang et al., 2019). During slack tide, the kelp canopy is vertically-orientated, meaning that only the width, rather the length, is captured by top-down imaging. Our findings indicate that at the high spatial resolution of our study, canopy length, as captured by side view imaging, has a greater impact on kelp canopy biomass than canopy width.

The canopy top-down view area showed a robust power relationship to density (r^2 = 0.676), indicating that the canopy width or "bushiness" correlates well with the density of sporophytes on the cultivation line. Monitoring this relationship is valuable for assessing density distribution across the farm, which can help to evaluate, for instance, the impacts of different seedling techniques, cultivation trials, or the influence of abiotic factors on kelp growth. Bell et al. (2020) illustrated the feasibility of repeated sporophyte density monitoring by detecting and classifying kelp juveniles along a horizontal cultivation line using side-view imaging from an AUV and machine learning processing.

Our canopy volume proxy was derived by multiplying the canopy side view area by the average width of its corresponding top-down view area. The canopy volume proxy showed a positive power relationship (r^2=0.681) to field-measured biomass, which was stronger than the power relationship (r^2 = 0.622) shown by manual length, but weaker than the power relationship (r^2 = 0.769) shown by side view area. This differs from the previously mentioned study by (Maimaitijiang et al., 2019), where UAV-based canopy volume estimations from high-density point clouds derived from photogrammetric stereo images showed a stronger correlation to biomass (r^2 = 0.849) than canopy height and projected basal area in predicting above-ground biomass (r^2=0.801 and 0.702, respectively). The authors reason that this could be explained by the volume estimations closer resemblance to the complex 3D structure of crop canopies. Unlike crop canopies, which are typically cultivated in fields over a continuous coverage or in structured rows, kelp canopies are cultivated on submerged substrates like lines or nets constantly affected by water currents. In our study, the kelp canopies are grown along horizontal cultivation lines, resulting in a distinctly different and arguably more complex 3D structure than crop canopies. More sophisticated techniques, such as stereo imaging, could be employed to improve the concept of our kelp canopy volume estimations. A preliminary investigation of the use of underwater stereo imaging to derive areal information about kelp canopies has been conducted by Gerlo et al. (2023), but to our knowledge, no RGB stereo imaging derived kelp canopy volume estimations have yet been performed.

4.2 Effect of environmental variables on SAM-derived segmentations

Our study observed a connection between measured IOPs ([*Chl a*] and turbidity) and image quality. The high image quality displayed during the two first field days (March 16th and March 29th) was likely due to high water visibility, resulting from low concentrations of the IOPs, such as *Chl a*, cDOM and TSM (Johnsen et al., 2020). As the concentration of the Chl *a* and turbidity increased from winter to summer, the observed image quality subsequently decreased. The image degradation resulted from increased light attenuation as photons were absorbed and/or scattered by the IOPs as they travelled through the water column (Kjerstad et al., 2014). As light attenuation increases exponentially with distance (Jerlov, 1951), the effect was amplified at the end of the growth cycle because a longer distance between the ROV and the kelp canopy is needed to capture the full length of a kelp that is reaching almost 2 m (Overrein et al., 2024).

The composition of IOP varies within water types (blue oceanic water versus greenish coastal waters) (Morel & Prieur, 1977), making underwater imaging effective at seaweed farms located in clear offshore waters and challenging in turbid, brackish coastal waters (Overrein et al., 2024). Our study was conducted in the waters of Frøya, a region known for its high productivity, with the occurrence of phytoplankton blooms from late March until June-July (Fragoso et al., 2021). This is aligned with the growth period of *S. latissima* at cultivation farms in the Trøndelag region (Førde et al., 2016), indicating that low water visibility can deteriorate underwater imaging quality during the later stages of the growth period.

Our image quality metric analysis illustrated a clear relationship between [*Chl a*] and image blur. In this study, high [*Chl a*] generally resulted in higher levels of Green Values, corresponding to the green hue present in *Chl a*-dominated waters (IOCCG, 2000). In general, a temporal trend was observed: Images from early in the season exhibited high Sharpness and Blue Values, with a distinct increase in Blur as the season advanced. This effect correlates with the rising levels of [*Chl a*] and turbidity measured, which cause increased absorption and scattering of underwater light. As the image quality metric calculations are a selection of the pre-set algorithms in the Encord Active library, it has to be taken into account that they serve a general purpose and are not explicitly customised for underwater images. By employing the same principles of pixel-based analysis, underwater image quality metrics aim to quantify image degradation typical for underwater environments, such as absorption, scattering, and colour attenuation (Lu et al., 2017). Subjective underwater quality metrics determined by visual inspection are considered to provide the most reliable results, but are expensive, time-consuming and impractical for real-time implementation and system integration (Han et al., 2020). The importance of objective image quality metrics in underwater environments is underscored as a critical component in underwater image processing, classification, and analysis, particularly for engineering and monitoring tasks (M. Yang & Sowmya, 2015).

Underwater image processing includes techniques such as underwater image enhancement, which involves algorithms for contrast enhancement and colour correction, aiming to reverse the image degradation caused by the water column (van de Weijer et al., 2007). While some models indirectly estimate the effects of the water column (Giardino et al., 2012), Rowan & Kalacska (2021) suggests that better results could be achieved by including directly measured parameters. Measuring the absorption and scattering coefficients during imaging can be used for pre-processing adjustments to restore an approximation of the original colours and contrast of the images (Kjerstad et al., 2014). Our imaging data are complemented by continuous measurements of [Chl a] and turbidity, but not cDOM. While restoring image quality was outside the scope of this study, future research should evaluate the costs associated with acquiring supplementary data for image enhancement against the potential benefits for subsequent analysis. An alternative approach to mitigating the problem of image degradation is to deploy inexpensive water sensors at the farm and use the data to optimise the timing of image surveys (Bell et al., 2020).

The SAM-derived segmentations aligned consistently with the observed kelp coverage to a satisfactory degree despite significant variations in image quality across the season. However, achieving satisfactory segmentation required a varying degree of human supervision. In conditions of high water visibility, the SAM predicted a satisfactory segmentation with few prompts (<5), likely because the high sharpness and contrast of the image enabled efficient edge detection. Under conditions of low water visibility, the SAM often over- or underestimated the observed kelp area, failing to accurately detect the boundary between kelp and background without the guidance of multiple prompts (>5) to achieve a satisfactory result. This interactive prompt engineering enables the SAM to adapt to a wide range of segmentation tasks (Kirillov et al., 2023), as demonstrated by its performance under distinctly different water conditions. The CV techniques used by Overrein et al. (2024) required tuning of individual parameters to each field day's varying image quality. While this provided adaptability for groups of images, it also made the process heavily reliant on human supervision. The lack of adjustability for individual images may have contributed to their significant underestimations of observed canopy areas in conditions of low water visibility.

4.3 Future perspectives for biomass estimation of cultivated kelp

Employing a mini-ROV as the sensor platform for our image surveys provided high-resolution data at a suitable spatial scale for our preliminary investigations. However, a ROV poses several constraints for large-scale monitoring, including the requirement for human intervention, restricted battery duration, and limited tether length (Sørensen et al., 2020). Given that seaweed farms already cover extensive areas and envision further upscaling (Skjermo et al., 2014), employing an ROV for underwater imaging is confined to subsections of the farm (Overrein et al., 2024). Studies within this spatial range could benefit from improvements in ROV autonomy. Automating tasks such as manoeuvring, inspection, and sampling could reduce the need for surface support, hence lower costs, while also making a significant progression toward the integration of AUVs and persistent underwater vehicles (Ludvigsen & Sørensen, 2016). Large-scale underwater monitoring would need to employ sensor platforms with a higher spatial coverage, such as AUVs. Although the cost of AUVs has limited their use in aquaculture operations, several small and cost-effective vehicles are entering the market, potentially revolutionising the collection of acoustic and colour imagery in the near future (Bell et al., 2020). Illustrating this potential, Stenius et al. (2022) propose a system for using AUVs to inspect seaweed farms automatically. In their validation trials, the AUV locates the pre-programmed GPS position of the farm and navigates along the cultivation lines using a side-scan sonar. Incorporating this setup for imaging surveys would allow us to gather data similar to our vertical footage and overcome current spatial limitations, enabling large-scale, autonomous and high-resolution underwater monitoring.

Biomass monitoring from underwater imaging of whole seaweed farms needs automated canopy detection and area segmentation. In its present form, the SAM require consistent manual supervision to provide satisfactory segmentations, making its low throughput a constraint for large-scale monitoring. In order to increase its performance and lower the need for human intervention, the foundational version of the SAM could be employed to train a model on our dataset of 108 canopy replicate images to be fine-tuned for that purpose. This process is conducted using a natural training algorithm that generates a sequence of prompts for each image and compares the model's predicted segmentation with the corresponding ground truth (Kirillov et al., 2023). The ground truth is a previously established "perfect" segmentation of the specified object(s). The model assesses its performance based on the percentage overlap between the two, represented as IoU. Based on this evaluation, the model iteratively refines its parameters to increase accuracy for segmentation tasks represented in the training data. The DeepLabv3+ (Chen et al., 2018) segmentation architecture was employed to develop a fine-tuned model for segmenting foreground objects in underwater images, significantly improving the model's standard mean IoU from 44.4% to 91.9% on a dataset of 300 *in situ* images (Drews-Jr et al., 2021). This deep learning architecture has also been employed to develop a fine-tuned model for segmenting kelp canopy coverage, achieving an IoU of 90% (Gerlo et al., 2023), thus demonstrating its potential for future automation in this field. To fine-tune the SAM on our dataset, establishing an objective ground truth is necessary. Even with human supervision, defining a "perfect" segmentation coverage would become challenging in images with significantly degraded quality and increased distance to the kelp, particularly common later in the season. An alternative approach to provide accurate ground truths is to simulate training data. Duarte et al. (2016) developed a simulator capable of transforming a clear image into a turbid underwater image of the same scene. This could be applied as it is or adjusted based on our IOP measurements to our high-water clarity images to generate training data for turbid conditions to fine-tune and evaluate the SAM model performance.

A challenge with underwater *in situ* mapping of kelp is its constant movement due to waves and tidal currents (Summers et al., 2022). We conducted our imaging survey under low wind conditions and during slack tide to minimise these forces on both the kelp and the ROV, aiming for consistently comparable results. As slack tides only occur during a limited time frame, employing this approach at a farm-level scale presents a challenge. The top-down view imaging is particularly sensitive to this issue, as even a slight drift in the kelp canopy could result in significant changes in the observed canopy area. Exploring alternative sensor platforms, resolution levels and tidal conditions is recommended to address this. As an alternative to the mini-ROV, an unmanned surface vehicle (USV) would enable comparable high-resolution top-down underwater imaging at a faster rate and over a larger area (Ludvigsen & Sørensen, 2016). Employing a low-flying UAV would further increase spatial coverage, but this would come at the cost of a lower spatial resolution and the added challenge of surface reflectance. Bell et al. (2020) highlights UAV imagery as the most viable solution for observing biomass quantity and condition of the floating surface canopies of cultivated *Macrocystis pyrifera* (giant kelp) at offshore farms. To investigate this approach for monitoring the submerged canopies of *S. latissima* at coastal locations, UAV surveys could be conducted during strong tidal currents when the kelp canopies are likely to be more horizontally oriented, thereby presenting a larger area closer to the water surface.

5 Conclusion

The canopy area estimations from side view images offered a more reliable proxy for biomass than manually measured lamina length, suggesting its potential to complement and replace traditional biomass estimations. While the canopy area estimations from top-down view images did not strongly correlate with biomass, it demonstrated a strong relationship to sporophyte density. Our preliminary results demonstrate the future potential of deriving structural canopy metrics from underwater imaging to gain new insights into *S. latissima* distribution and growth patterns along cultivation lines.

The evaluation of our image dataset demonstrated a clear impact of Chl *a* and turbidity concentrations on observed image quality, with high concentrations resulting in a green hue and reduced sharpness. Despite this, the SAM consistently achieved a satisfactory accuracy in its kelp canopy segmentations, even from substantially degraded images. However, it required additional manual supervision. The level of accuracy could be further improved and quantified using machine learning and underwater image enhancement techniques.

Our study has continued the work of Overrein et al. (2024), and our results support their claim that CV-derived area estimations from underwater imagery of kelp canopies can serve as a robust proxy for canopy biomass. Our use of mini-ROV imaging surveys facilitates non-destructive and repeatable underwater monitoring. We have built upon their original approach by incorporating top-down view imaging, deriving a canopy volume proxy, quantifying image quality metrics and utilising the SAM for canopy area segmentation. Our findings indicate that using the SAM, a promptable foundation model for image segmentation, for canopy area segmentations increased the adaptability, efficiency and accuracy compared to previously employed conventional segmentation techniques. To further reduce the need for manual supervision, we have released together with this thesis our dataset of 108 canopy replicate images and its corresponding segmentations, which can be used to fine-tune a model specialised for canopy segmentations in the waters of Frøya.

This study presents a novel step toward automated and large-scale *in situ* monitoring of cultivated kelp canopies. However, our current approach faces several constraints, such as operational limitations in the field and semi-automatic processing. We envision that our work can serve as a foundation to overcome these limitations by implementing autonomous sensory systems and advanced machine learning processing.

References

Albrecht, M. (2023). A Norwegian seaweed utopia? Governmental narratives of coastal communities, upscaling, and the industrial conquering of ocean spaces. *Maritime Studies*, *22*(3), 1–12. https://doi.org/10.1007/S40152-023-00324-2/METRICS

Albrecht, M., & Lukkarinen, J. (2020). Blue bioeconomy localities at the margins: Reconnecting Norwegian seaweed farming and Finnish small-scale lake fisheries with blue policies. *Https://Doi.Org/10.1177/2399654420932572*, *38*(7–8), 1465–1483. https://doi.org/10.1177/2399654420932572

Ashraf, S., Brabyn, L., Hicks, B. J., & Collier, K. (2010). Satellite remote sensing for mapping vegetation in New Zealand freshwater environments: A review. *New Zealand Geographer*, *66*(1), 33–43. https://doi.org/10.1111/J.1745-7939.2010.01168.X

Bell, T. W., Nidzieko, N. J., Siegel, D. A., Miller, R. J., Cavanaugh, K. C., Nelson, N. B., Reed, D. C., Fedorov, D., Moran, C., Snyder, J. N., Cavanaugh, K. C., Yorke, C. E., & Griffith, M. (2020). The Utility of Satellites and Autonomous Remote Sensing Platforms for Monitoring Offshore Aquaculture Farms: A Case Study for Canopy Forming Kelps. *Frontiers in Marine Science*, *7*, 520223. https://doi.org/10.3389/FMARS.2020.520223/BIBTEX

Bewley, M., Nourani-Vatani, N., Friedman, A., Bewley, M. S., Douillard, B., Nourani-Vatani, N., Friedman, A., Pizarro, O., & Williams, S. B. (2012). Automated species detection: An experimental approach to kelp detection from sea-floor AUV images. *Researchgate.NetM Bewley, B Douillard, N Nourani-Vatani, A Friedman, O Pizarro, S WilliamsProc Australas Conf Rob Autom, 2012•researchgate.Net*. https://www.researchgate.net/profile/Michael-Bewley/publication/283257248_Automated_species_detection_An_experimental_approach_to_kelp_detection_from_sea-floor_AUV_images/links/562f472108aef25a244554eb/Automated-species-detection-An-experimental-approach-to-kelp-detection-from-sea-floor-AUV-images.pdf

Broch, O. J., Alver, M. O., Bekkby, T., Gundersen, H., Forbord, S., Handå, A., Skjermo, J., & Hancke, K. (2019). The kelp cultivation potential in coastal and offshore regions of Norway. *Frontiers in Marine Science*, *5*(JAN), 429801. https://doi.org/10.3389/FMARS.2018.00529/BIBTEX

Cai, J., Lovatelli, A., Aguilar-Manjarrez, J., Cornish, L., Dabbadie, L., Desrochers, A., Diffey, S., Garrido Gamarro, E., Geehan, J., & Hurtado, A. (2021). Seaweeds and microalgae: an overview for unlocking their potential in global aquaculture development. *FAO Fisheries and Aquaculture Circular*, *1229*.

Cavanaugh, K. C., Bell, T., Costa, M., Eddy, N. E., Gendall, L., Gleason, M. G., Hessing-Lewis, M., Martone, R., McPherson, M., Pontier, O., Reshitnyk, L., Beas-Luna, R., Carr, M., Caselle, J. E., Cavanaugh, K. C., Flores Miller, R., Hamilton, S., Heady, W. N., Hirsh, H. K., … Schroeder, S. B. (2021). A Review of the Opportunities and Challenges for Using Remote Sensing for Management of Surface-Canopy Forming

Kelps. *Frontiers in Marine Science*, *8*, 753531. https://doi.org/10.3389/FMARS.2021.753531/BIBTEX

Chen, L. C., Zhu, Y., Papandreou, G., Schroff, F., & Adam, H. (2018). Encoder-decoder with atrous separable convolution for semantic image segmentation. *Lecture Notes in Computer Science (Including Subseries Lecture Notes in Artificial Intelligence and Lecture Notes in Bioinformatics)*, *11211 LNCS*, 833–851. https://doi.org/10.1007/978-3-030-01234-2_49/TABLES/7

Clarke, R., & Gorley, R. N. (2014). *PRIMER-e* (7).

Cohen, J. H., Berge, J., Moline, M. A., Johnsen, G., Zolich, A. P., Cohen, J. H., Moline, M. A., Berge, J., Johnsen, G., & Zolich, A. P. (2020). Light in the Polar Night. *Advances in Polar Ecology*, *4*, 37–66. https://doi.org/10.1007/978-3-030-33208-2_3

Communication from the Commission: Towards a Strong and Sustainable EU Algae Sector - European Commission (2023). https://oceans-and-fisheries.ec.europa.eu/publications/communication-commission-towards-strong-and-sustainable-eu-algae-sector_en

Davis, K. F., Gephart, J. A., Emery, K. A., Leach, A. M., Galloway, J. N., & D'Odorico, P. (2016). Meeting future food demand with current agricultural resources. *Global Environmental Change*, *39*, 125–132. https://doi.org/10.1016/J.GLOENVCHA.2016.05.004

Dillehay, T. D., Ramírez, C., Pino, M., Collins, M. B., Rossen, J., & Pino-Navarro, J. D. (2008). Monte Verde: Seaweed, food, medicine, and the peopling of South America. *Science*, *320*(5877), 784–786. https://doi.org/10.1126/SCIENCE.1156533

Directorate of Fisheries. (2024). *Akvakulturstatistikk: alger*. https://www.fiskeridir.no/Akvakultur/Tall-og-analyse/Akvakulturstatistikk-tidsserier/Alger

Drews-Jr, P., Souza, I. de, Maurell, I. P., Protas, E. V., & Silvia, S. S. (2021). Underwater image segmentation in the wild using deep learning. *Journal of the Brazilian Computer Society*, *27*(1), 1–14. https://doi.org/10.1186/S13173-021-00117-7/TABLES/1

Duarte, A., Codevilla, F., Gaya, J. D. O., & Botelho, S. S. C. (2016). A dataset to evaluate underwater image restoration methods. *OCEANS 2016 - Shanghai*. https://doi.org/10.1109/OCEANSAP.2016.7485524

Duarte, C. M., Bruhn, A., & Krause-Jensen, D. (2021). A seaweed aquaculture imperative to meet global sustainability targets. *Nature Sustainability 2021 5:3*, *5*(3), 185–193. https://doi.org/10.1038/s41893-021-00773-9

Encord. (2023). *Encord Active* (0.1.84).

Ene, L. T., Gobakken, T., Andersen, H. E., Næsset, E., Cook, B. D., Morton, D. C., Babcock, C., & Nelson, R. (2018). Large-area hybrid estimation of aboveground biomass in interior Alaska using airborne laser scanning data. *Remote Sensing of Environment*, *204*, 741–755. https://doi.org/10.1016/J.RSE.2017.09.027

Ervik, H., Finne, T. E., & Jenssen, B. M. (2018). Toxic and essential elements in seafood from Mausund, Norway. *Environmental Science and Pollution Research*, *25*(8), 7409–7417. https://doi.org/10.1007/S11356-017-1000-4/TABLES/6

Førde, H., Forbord, S., Handå, A., Fossberg, J., Arff, J., Johnsen, G., & Reitan, K. I. (2016). Development of bryozoan fouling on cultivated kelp (Saccharina latissima) in Norway. *Journal of Applied Phycology*, *28*(2), 1225–1234. https://doi.org/10.1007/S10811-015-0606-5/FIGURES/9

Føre, M., & Alver, M. O. (2023). Precision Aquaculture. *Encyclopedia of Smart Agriculture Technologies*, 1–12. https://doi.org/10.1007/978-3-030-89123-7_26-1

Fragoso, G. M., Johnsen, G., Chauton, M. S., Cottier, F., & Ellingsen, I. (2021). Phytoplankton community succession and dynamics using optical approaches. *Continental Shelf Research*, *213*, 104322. https://doi.org/10.1016/J.CSR.2020.104322

Free, G., Bresciani, M., Trodd, W., Tierney, D., O'Boyle, S., Plant, C., & Deakin, J. (2020). Estimation of lake ecological quality from Sentinel-2 remote sensing imagery. *Hydrobiologia*, *847*(6), 1423–1438. https://doi.org/10.1007/S10750-020-04197-Y

Gao, Y., Li, Q., Wang, S., & Gao, J. (2018). Adaptive neural network based on segmented particle swarm optimization for remote-sensing estimations of vegetation biomass. *Remote Sensing of Environment*, *211*, 248–260. https://doi.org/10.1016/J.RSE.2018.04.026

Gerlo, J., Kooijman, D. G., Wieling, I. W., Heirmans, R., & Vanlanduit, S. (2023). Seaweed Growth Monitoring with a Low-Cost Vision-Based System. *Sensors 2023, Vol. 23, Page 9197*, *23*(22), 9197. https://doi.org/10.3390/S23229197

Giardino, C., Candiani, G., Bresciani, M., Lee, Z., Gagliano, S., & Pepe, M. (2012). BOMBER: A tool for estimating water quality and bottom properties from remote sensing images. *Computers & Geosciences*, *45*, 313–318. https://doi.org/10.1016/J.CAGEO.2011.11.022

Han, M., Lyu, Z., Qiu, T., & Xu, M. (2020). A Review on Intelligence Dehazing and Color Restoration for Underwater Images. *IEEE Transactions on Systems, Man, and Cybernetics: Systems*, *50*(5), 1820–1832. https://doi.org/10.1109/TSMC.2017.2788902

Hwang, E. K., Yotsukura, N., Pang, S. J., Su, L., & Shan, T. F. (2019). Seaweed breeding programs and progress in eastern Asian countries. *Phycologia*, *58*(5), 484–495. https://doi.org/10.1080/00318884.2019.1639436

IOCCG. (2000). Remote Sensing of Ocean Colour in Coastal, and Other Optically-Complex, Waters. *Reports of the International Ocean-Colour Coordinating Group*, *3*. https://doi.org/10.25607/OBP-95

Jerlov, N. G. (1951). Optical studies of ocean water. *Rept. Swedish Deep-Sea Exped.*, *3*, 1–59.

Jin, R., Ye, Z., Chen, S., Gu, J., He, J., Huang, L., Christakos, G., Agusti, S., Duarte, C. M., & Wu, J. (2023). Accurate mapping of seaweed farms with high-resolution imagery in China. *Geocarto International*, *38*(1). https://doi.org/10.1080/10106049.2023.2203114

Johnsen, G., Leu, E., Gradinger, R., Johnsen, G., Leu, E., & Gradinger, R. (2020). Marine Micro- and Macroalgae in the Polar Night. *Advances in Polar Ecology*, *4*, 67–112. https://doi.org/10.1007/978-3-030-33208-2_4

Johnsen, G., Mogstad, A. A., Berge, J., Cohen, J. H., Johnsen, G., Mogstad, A. A., Berge, J., & Cohen, J. H. (2020). Operative Habitat Mapping and Monitoring in the Polar Night. *Advances in Polar Ecology*, *4*, 277–305. https://doi.org/10.1007/978-3-030-33208-2_10

Kim, J. K., Yarish, C., Hwang, E. K., Park, M., Kim, Y., Kim, J. K., Yarish, C., Hwang, E. K., Park, M., & Kim, Y. (2017). Seaweed aquaculture: cultivation technologies, challenges and its ecosystem services. *Algae*, *32*(1), 1–13. https://doi.org/10.4490/ALGAE.2017.32.3.3

Kirillov, A., Mintun, E., Ravi, N., Mao, H., Rolland, C., Gustafson, L., Xiao, T., Whitehead, S., Berg, A. C., Lo, W.-Y., Dollár, P., & Girshick, R. (2023). *Segment Anything*.

Kjerstad, I., Bakken, T., & Sørensen, A. (2014). Underwater Imaging and the effect of Inherent Optical Properties on image quality. *82*. https://ntnuopen.ntnu.no/ntnu-xmlui/handle/11250/245550

Kraan, S. (2020). Seaweed resources, collection, and cultivation with respect to sustainability. *Sustainable Seaweed Technologies: Cultivation, Biorefinery, and Applications*, 89–102. https://doi.org/10.1016/B978-0-12-817943-7.00003-2

Krause-Jensen, D., & Duarte, C. M. (2016). Substantial role of macroalgae in marine carbon sequestration. *Nature Geoscience 2016 9:10*, *9*(10), 737–742. https://doi.org/10.1038/ngeo2790

Lauzon-Guay, J. S., Ugarte, R. A., Morse, B. L., & Robertson, C. A. (2021). Biomass and height of Ascophyllum nodosum after two decades of continuous commercial harvesting in eastern Canada. *Journal of Applied Phycology*, *33*(3), 1695–1708. https://doi.org/10.1007/S10811-021-02427-X/FIGURES/8

Lee, H., Brown, C., Seo, B., Holman, I., Audsley, E., Cojocaru, G., & Rounsevell, M. (2019). Implementing land-based mitigation to achieve the Paris Agreement in Europe requires food system transformation. *Environmental Research Letters*, *14*(10), 104009. https://doi.org/10.1088/1748-9326/ab3744

Lloyd's Register Foundation. (2020). *Seaweed Manifesto | UN Global Compact*. https://unglobalcompact.org/library/5743

Lu, H., Li, Y., Zhang, Y., Chen, M., Serikawa, S., & Kim, H. (2017). Underwater Optical Image Processing: A Comprehensive Review. *Mobile Networks and Applications*, *22*(6), 1204–1211. https://doi.org/10.1007/s11036-017-0863-4

Ludvigsen, M., & Sørensen, A. J. (2016). Towards integrated autonomous underwater operations for ocean mapping and monitoring. *Annual Reviews in Control*, *42*, 145–157. https://doi.org/10.1016/J.ARCONTROL.2016.09.013

Mac Monagail, M., Cornish, L., Morrison, L., Araújo, R., & Critchley, A. T. (2017). Sustainable harvesting of wild seaweed resources. *European Journal of Phycology*, *52*(4), 371–390. https://doi.org/10.1080/09670262.2017.1365273

Maimaitijiang, M., Sagan, V., Sidike, P., Maimaitiyiming, M., Hartling, S., Peterson, K. T., Maw, M. J. W., Shakoor, N., Mockler, T., & Fritschi, F. B. (2019). Vegetation Index Weighted Canopy Volume Model (CVMVI) for soybean biomass estimation from Unmanned Aerial System-based RGB imagery. *ISPRS Journal of Photogrammetry and Remote Sensing*, *151*, 27–41. https://doi.org/10.1016/J.ISPRSJPRS.2019.03.003

McGlamery, B. L. (1980). A Computer Model For Underwater Camera Systems. *Other Conferences*, *0208*, 221–231. https://doi.org/10.1117/12.958279

Meltytech LLC. (2024). *Shotcut* (23.12).

Microsoft. (2024). *Excel* (2403).

Morel, A., & Prieur, L. (1977). Analysis of variations in ocean color1. *Limnology and Oceanography*, *22*(4), 709–722. https://doi.org/10.4319/LO.1977.22.4.0709

Olafsen, T., Winther, U., Olsen, Y., & Skjermo, J. (2012). Value created from productive oceans in 2050. *SINTEF Fisheries and Aquaculture*, *83*.

Overrein, M. M., Tinn, P., Aldridge, D., Johnsen, G., & Fragoso, G. M. (2024). Biomass estimations of cultivated kelp using underwater RGB images from a mini-ROV and computer vision approaches. *Frontiers in Marine Science*, *11*. https://doi.org/10.3389/fmars.2024.1324075

Rowan, G. S. L., & Kalacska, M. (2021). A Review of Remote Sensing of Submerged Aquatic Vegetation for Non-Specialists. *Remote Sensing 2021, Vol. 13, Page 623*, *13*(4), 623. https://doi.org/10.3390/RS13040623

Saether, M., Diehl, N., Monteiro, · Cátia, Li, H., Niedzwiedz, S., Bertille Burgunter-Delamare, ·, Scheschonk, L., Bischof, K., & Forbord, S. (2024). The sugar kelp Saccharina latissima II: Recent advances in farming and applications. *Journal of Applied Phycology 2024*, 1–33. https://doi.org/10.1007/S10811-024-03213-1

Skagseth, O., Drinkwater, K. F., & Terrile, E. (2011). Wind- and buoyancy-induced transport of the Norwegian Coastal Current in the Barents Sea. *Journal of Geophysical Research: Oceans*, *116*(C8), 8007. https://doi.org/10.1029/2011JC006996

Skjermo, J., Aasen, I. M., Arff, J., Broch, O. J., Carvajal, A., Christie, H., Forbord, S., Olsen, Y., Reitan, I., Rustad, T., Sandquist, J., Solbakken, R., Steinhovden, K. B., Wittgens, B., Wolff, R., & Handå, A. (2014). *A new Norwegian bioeconomy based on cultivation and processing of seaweeds: Opportunities and R&D needs*.

Sørensen, A. J., Ludvigsen, M., Norgren, P., Ødegård, Ø., Cottier, F., Sørensen, A. J., Ludvigsen, · M, Norgren, · P, & Ødegård, Ø. (2020). Sensor-Carrying Platforms. *Advances in Polar Ecology*, *4*, 241–275. https://doi.org/10.1007/978-3-030-33208-2_9

Steen, H., Moy, F. E., Bodvin, T., & Husa, V. (2016). Regrowth after kelp harvesting in Nord-Trøndelag, Norway. *ICES Journal of Marine Science*, *73*(10), 2708–2720. https://doi.org/10.1093/ICESJMS/FSW130

Stenius, I., Folkesson, J., Bhat, S., Sprague, C. I., Ling, L., Özkahraman, Ö., Bore, N., Cong, Z., Severholt, J., Ljung, C., Arnwald, A., Torroba, I., Gröndahl, F., & Thomas, J. B. (2022). A System for Autonomous Seaweed Farm Inspection with an Underwater Robot. *Sensors 2022, Vol. 22, Page 5064*, *22*(13), 5064. https://doi.org/10.3390/S22135064

Stévant, P., Rebours, C., & Chapman, A. (2017). Seaweed aquaculture in Norway: recent industrial developments and future perspectives. *Aquaculture International*, *25*(4), 1373–1390. https://doi.org/10.1007/S10499-017-0120-7/FIGURES/1

Summers, N., Johnsen, G., Mogstad, A., Løvås, H., Fragoso, G., & Berge, J. (2022). Underwater Hyperspectral Imaging of Arctic Macroalgal Habitats during the Polar Night Using a Novel Mini-ROV-UHI Portable System. *Remote Sensing 2022, Vol. 14, Page 1325*, *14*(6), 1325. https://doi.org/10.3390/RS14061325

Tiller, R. G., Hansen, L., Richards, R., & Strand, H. (2015). Work segmentation in the Norwegian salmon industry: The application of segmented labor market theory to work migrants on the island community of Frøya, Norway. *Marine Policy*, *51*, 563–572. https://doi.org/10.1016/J.MARPOL.2014.10.001

van de Weijer, J., Gevers, T., & Gijsenij, A. (2007). Edge-based color constancy. *IEEE Transactions on Image Processing*, *16*(9), 2207–2214. https://doi.org/10.1109/TIP.2007.901808

Wang, C., Nie, S., Xi, X., Luo, S., Sun, X., Zhang, J., Lin, X., Baghdadi, N., Gloaguen, R., & Thenkabail, P. S. (2016). Estimating the Biomass of Maize with Hyperspectral and LiDAR Data. *Remote Sensing 2017, Vol. 9, Page 11*, *9*(1), 11. https://doi.org/10.3390/RS9010011

Wilson, C. J. (2011). *The acoustic ecology of submerged macrophytes*. http://hdl.handle.net/2152/ETD-UT-2011-12-4742

World Bank. (2023). *Global Seaweed: New and Emerging Markets Report, 2023*. http://hdl.handle.net/10986/40187

Yan, Y. (2023). Machine Learning Fundamentals. *Encyclopedia of Smart Agriculture Technologies*, 1–7. https://doi.org/10.1007/978-3-030-89123-7_69-1

Yang, M., & Sowmya, A. (2015). An Underwater Color Image Quality Evaluation Metric. *IEEE Transactions on Image Processing*, *24*(12), 6062–6071. https://doi.org/10.1109/TIP.2015.2491020

Yang, X., Zhang, S., Liu, J., Gao, Q., Dong, S., & Zhou, C. (2020). Deep learning for smart fish farming: applications, opportunities and challenges. *Reviews in Aquaculture*, *13*(1), 66–90. https://doi.org/10.1111/raq.12464

Yong, W. T. L., Thien, V. Y., Rupert, R., & Rodrigues, K. F. (2022). Seaweed: A potential climate change solution. *Renewable and Sustainable Energy Reviews*, *159*, 112222. https://doi.org/10.1016/J.RSER.2022.112222

NTNU

Norwegian University of
Science and Technology